Supplemental Figure 7

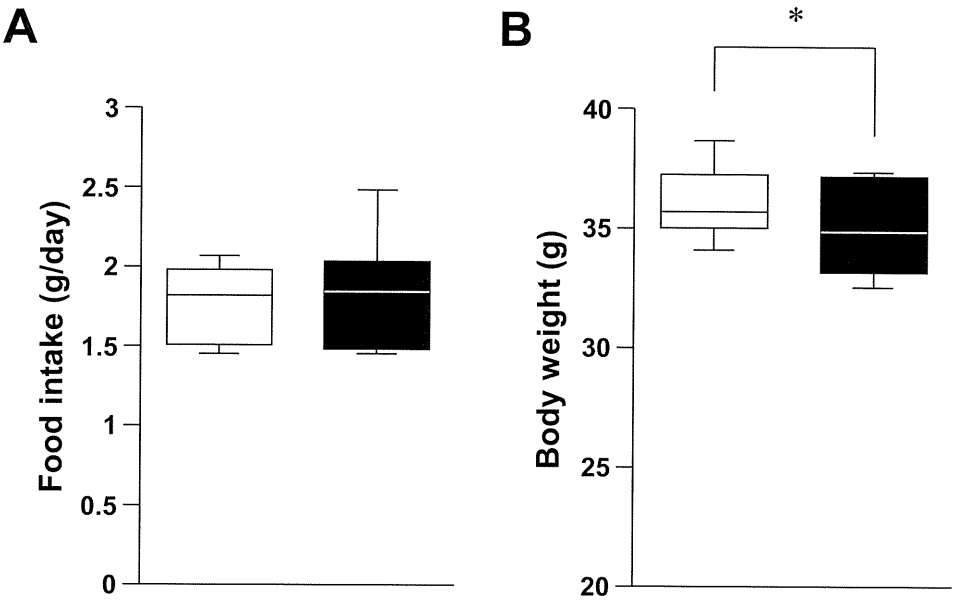

Supplemental Figure 8

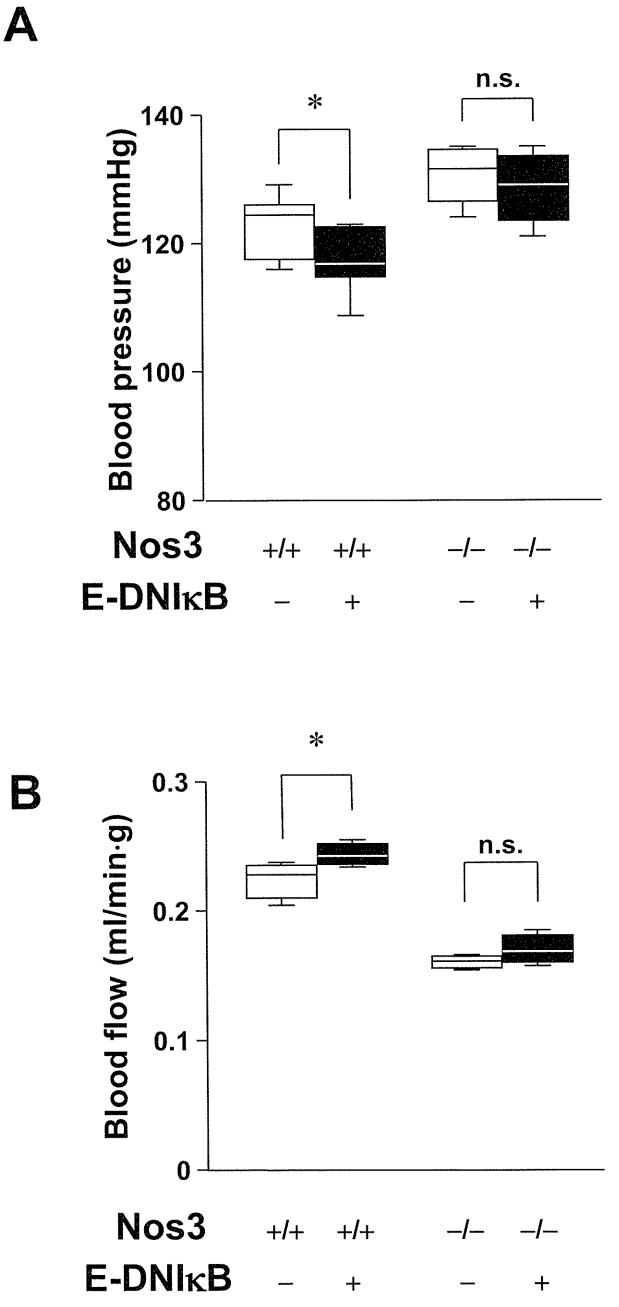

Supplemental Figure 9

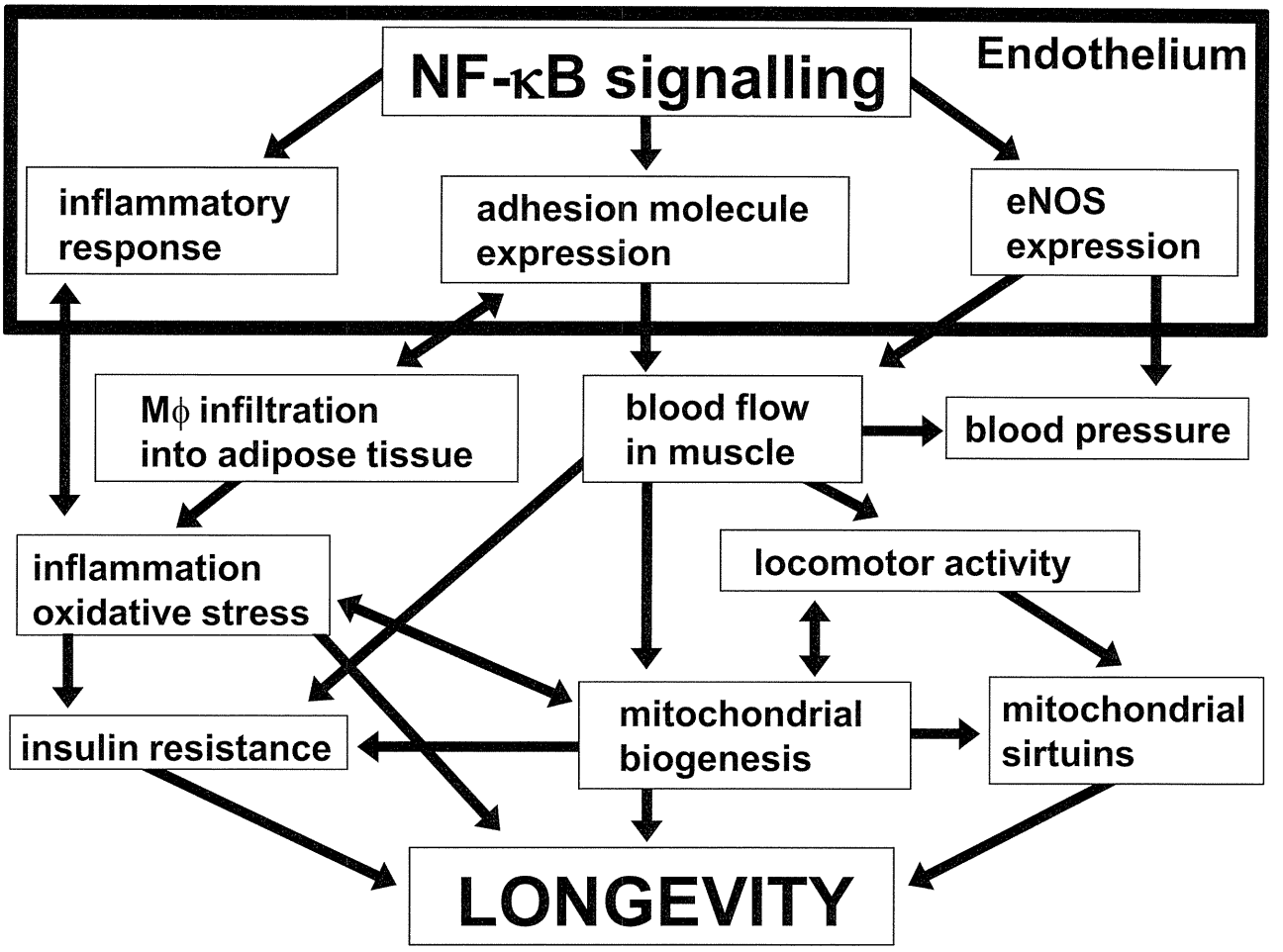

Supplemental Table 1

Probe	Primer 1	Primer 2
VCAM-1	GGA AGCTGGAACGAA GTA	CAATCTCCAGCCTGTAAACT
E-selectin	CATCGTCCTCATTGCTCTA	AGACGTTGTAAGAAGGCAC
eNOS	ATGTTTGTCTGCGGCGATGT	ATGTCCTCGTGGTAGCGTTG
F4/80	CATCATGGCATACCTGTTCAC	GAATGGGAGCTA AGGTCAGTC
iNOS	CAGCTGGGCTGTACAAACCTT	CATTGGAAGTGAAGCGTTTCG
Cytochrome C	GATTCTCTTACACAGATGCC	CTTCTTCTTAATTCCAGCGA
UCP-3	ATGCTGAAGATGGTGGCTC	CCGCAGTACCTGGACTTT
MCAD	TCGAAAGCGGCTCACAAGCAG	CACCGCAGCTTTCCGGAATGT
Nampt	AACGAAAGAGGATGGAACTAC	TACCAGGACTGAACAAGAATA
SIRT3	CTGCAAGGTTCCTACTCCA	CTTCGAGGACTCAGAACG
TNF-α	AGGTCAACGTTTCTGATTA	GGGTGGGTAGAATG
PEPCK	TTGCCTGGATGAAGTTTGAT	GGCATTTGGATTTGTCTTCACT
G6Pase	AAAGAGACTGTGGGCATCAATC	AATGCCTGACAAGACTCCAGCC
Tie2	CTTGTTGGCGTTTCTGATTA	TGATGTCATTCCAGTCAAGC
VEGF	TCATGCGGATCAAACCTCA	TTTCTGGCTTTGTTCTGTCTT
ICAM-1	GCTGCTACCTGCACTTTG	GGATGGATGGATACCTGA
Glutathion peroxidase	TGCAGAAGCGTCTGGGACCT	GGTCGGACGTACTTGAGGGA
MnSOD	GGTCGCTTACAGATTGCT	CTCCCAGTTGATTACATTCC
Alpha-actin	CAAATGCTTCTAAGTCCC	CCACGAGTAACAAATCAAAG
Beta-actin	TTGTAACCAACTGGGACGATATGG	GATCTTGATCTTCATGGTGCTAGG

Available at www.sciencedirect.com

Metabolism

www.metabolismjournal.com

Atf6α-null mice are glucose intolerant due to pancreatic β-cell failure on a high-fat diet but partially resistant to diet-induced insulin resistance

Masahiro Usui[a], *Suguru Yamaguchi*[a,b], *Yasuhiro Tanji*[a], *Ryu Tominaga*[a], *Yasushi Ishigaki*[a], *Manabu Fukumoto*[c], *Hideki Katagiri*[d], *Kazutoshi Mori*[e], *Yoshitomo Oka*[a], *Hisamitsu Ishihara*[a,b,*]

[a] *Division of Molecular Metabolism and Diabetes, Tohoku University Graduate School of Medicine, Sendai 980-8575, Japan*
[b] *Division of Diabetes and Metabolism, Nihon University School of Medicine, Tokyo 173-8610, Japan*
[c] *Department of Pathology, Institute of Development, Aging and Cancer, Tohoku University Graduate School of Medicine, Sendai 980-8575, Japan*
[d] *Department of Metabolic Diseases, Center for Metabolic Diseases, Tohoku University Graduate School of Medicine, Sendai 980-8575, Japan*
[e] *Department of Biophysics, Graduate School of Science, Kyoto University, Kyoto 606-8502, Japan*

ARTICLE INFO

Article history:
Received 1 September 2011
Accepted 5 January 2012

ABSTRACT

Activating transcription factor 6α (ATF6α) is essential for the endoplasmic reticulum (ER) stress response. Since recent studies suggested that ER stress is involved in the pathogenesis of type 2 diabetes mellitus, we have analyzed *Atf6α*-null (*Atf6α*$^{-/-}$) mice challenged with metabolic overload or genetic manipulations. *Atf6α*$^{-/-}$ mice were fed a high-fat diet to create diet-induced obese (DO) mice, and were subjected to examination of glucose homeostasis with biochemical and morphological analysis of the pancreatic β-cell and liver tissues. *Atf6α*-null mice were also crossed with genetic models of diabetes caused either by insulin resistance (Agouti obese mice) or by impaired insulin secretion (*Ins2*$^{WT/C96Y}$ mice). *Atf6α*$^{-/-}$ DO mice were less glucose tolerant with blunted insulin secretion compared to littermates on a high-fat diet. Pancreatic insulin content was lower in *Atf6α*$^{-/-}$ DO mice with the swollen β-cell ER, a typical feature of cells with ER stress. In the liver of *Atf6α*$^{-/-}$ DO mice, XBP-1 splicing was increased, suggesting that higher ER stress was present. ATF6-deficient mice showed increased mRNA expressions of glucose-6-phosphatase and SREBP1c associated with a tendency for a higher degree of steatosis in the liver. However, *Atf6α*$^{-/-}$ DO mice exhibited higher insulin sensitivity with lower serum triglyceride levels. Similar phenotypes were observed in ATF6α-deficient Agouti mice. In addition, ATF6α-deficiency accelerated reduction in pancreatic insulin content in *Ins2*$^{WT/C96Y}$ mice. These data suggested that ATF6α contributes to both prevention and promotion of diabetes; it

Abbreviations: ATF6α, activating transcription factor 6α; BW, body weight; cDNA, complementary DNA; DO, diet-induced obese; eIF2α, eukaryotic initiation factor 2; ER, endoplasmic reticulum; G6Pase, glucose-6-phosphatase; GRP78, 78 kDa glucose-regulated protein; HFD, high-fat diet; IPGTT, intraperitoneal glucose tolerance test; ITT, intraperitoneal insulin tolerance test; IRE1, inositol requiring enzyme 1; PERK, PKR (double-stranded-RNA-dependent protein kinase)-like ER kinase; TG, triglyceride; UPR, unfolded protein response; VLDL, very low-density lipoprotein; WT, wild-type; XBP, X-box binding protein.

Authors' contributions: H.K., K.M., Y.O. and H.I. designed the research; M.U., S.Y., Y.T., R.T., and Y.I. performed the research; S.Y., Y.I., M.F., S.Y., and H.I. analyzed the data; M.U., Y.O., and H.I. wrote the paper.

* *Corresponding author.* Hisamitsu Ishihara, Division of Diabetes and Metabolism, Nihon University School of Medicine, Itabashi-ku, Tokyo 173-8610, Japan. Tel. +81 3 3972 8245; fax. +81 3 3972 8245.
E-mail address: ishihara.hisamitsu@nihon-u.ac.jp (H. Ishihara).

0026-0495/$ – see front matter
doi:10.1016/j.metabol.2012.01.004

protects β-cells from ER stress and suppresses hepatosteatosis, but plays a role in the development of hyperlipidemia and insulin resistance.

1. Introduction

Glucose homeostasis is maintained through fine regulation of insulin secretion from pancreatic β-cells and glucose production from the liver as well as glucose disposal into muscle and adipose tissues [1]. Recent studies have shown decreased pancreatic β-cell mass to be a common feature of subjects with type 2 diabetes mellitus (T2DM) [2-4]. Stress-mediated apoptosis is considered as one of the causes of β-cell loss. Pancreatic β-cells are especially vulnerable to endoplasmic reticulum (ER) stress [5,6] because of continuous and abundant production of insulin. In addition, ER stress and the activation of related stress signaling pathways are suggested to be an important mechanism underlying insulin resistance [7,8]. Recent studies showed that ER stress is present in adipose and liver tissues in obese humans [9-11].

ER stress is triggered when the amount of unfolded and misfolded proteins exceeds the folding capacity of the ER. This protein folding stress is recognized by three ER-resident transmembrane proteins, PERK (PKR (double-stranded-RNA-dependent protein kinase)-like ER kinase), IRE1 (inositol requiring enzyme 1) and ATF6α (activating transcription factor 6α). These ER stress sensor proteins initiate a series of signaling cascades known as the unfolded protein response (UPR) [12,13]. The UPR reduces ER stress in two ways, one of which is by reduction in ER protein load. This reduction is mediated by activation of PERK, which phosphorylates α subunit of eukaryotic translation initiation factor eIF2 (eIF2α), resulting in inhibition of global protein synthesis [14]. Another means to cope with ER stress is to increase protein folding capacity and to enhance activity of protein degradation. PERK-mediated inhibition of global protein synthesis paradoxically increases expression of ATF4. Activation of IRE1 leads to generation of an active form of transcription factor XBP-1 (X-box binding protein-1). These transcription factors together with ATF6α orchestrate transcriptional induction of specific genes which facilitate folding or degradation of misfolded proteins. Essential roles of PERK and IRE1α in cell survival have been established mainly through studies using *Perk*-null [15] and *Ire1α*-null [16] cells and mice. Furthermore, mutations of the *EIF2AK3* gene encoding PERK in humans cause Wolcott–Rallison syndrome with diabetes mellitus in early infancy [17], demonstrating an essential importance of PERK signaling in β-cells.

In contrast to these sub-pathways of the UPR, studies of the ATF6α-mediated pathway in the cell or organ physiology have recently been commenced. ATF6α is a type II transmembrane glycoprotein located on the ER membrane. In response to ER stress, ATF6α is cleaved and the N-terminus 50 kDa protein moves to the nucleus. Once in the nucleus ATF6α binds to the ER stress response elements in ER stress genes, which include molecular chaperones GRP78 and GRP94, augmenting ER capacity to assist folding of secretory and membrane proteins [13,18]. Recently, *Atf6α* knockout mice were generated [19,20]. Using cells from these mice, ATF6α was revealed to function as a critical regulator of ER quality control proteins.

In humans, expression of GRP78, a downstream effecter of ATF6α, was reportedly increased in T2DM β-cells [21]. Expressions of molecular chaperones downstream of ATF6α were also shown to be augmented in human adipose tissue and liver with obesity [10,11]. Furthermore, the ATF6α-Met67Val substitution with increased intrinsic activity was found to cause elevation in plasma cholesterol levels [22]. Several single nucleotide polymorphisms in the *ATF6α* gene were found to associate with T2DM [23-25], although a lack of association between genetic polymorphisms in the locus and glucose metabolism was also recently reported [26]. These data suggest an important role of ATF6α in development of obesity and T2DM. However, the causal relationship is not clear nor has the role of ATF6α been established in whole body glucose homeostasis. Therefore, in this study, we have analyzed glucose homeostasis in *Atf6α*-null mice challenged with metabolic overload or genetic manipulations.

2. Materials and methods

2.1. Animals

The Tohoku University Institutional Animal Care and Use Committee approved all animal experiments. Generation of *Atf6α*-null mice was described previously [20]. Heterozygous *Atf6α* knockout mice ($Atf6\alpha^{+/-}$) were backcrossed to female wild-type C57BL/6J mice eight times. Homozygous knockout mice were produced by intercrossing male and female heterozygotes. Genotyping for *Atf6α* knockout allele was performed using the forward primer 5′-CTTCTGAGGCGGAAAGAACCAGCTG-3′ and the reverse primer 5′-TTTGCAAGTC CAATGGGCC TCTC-3′. Reverse transcription PCR for detecting expression of *Atf6α* mRNA was conducted using primers 5′-CCAACAGAAAGCCGCATT-3′ and 5′-TGGACAGCCATCAGCTGA GA-3′. $Ins2^{WT/C96Y}$ (Akita) mice (C57BL/6J background, [27]) were purchased from Charles River. Male $Ins2^{WT/C96Y}$ mice were mated with female $Atf6\alpha^{-/-}$ mice to generate $Atf6\alpha^{+/-}Ins2^{WT/C96Y}$ mice which were further mated with female $Atf6\alpha^{-/-}$ to produce $Atf6\alpha^{-/-}Ins2^{WT/C96Y}$ mice. Genotyping for $Ins2^{WT/C96Y}$ mice was as described previously [27]. C57BL/6J Ham Slc-$A^{y/+}$(A^y) mice were obtained from Japan SLC. Male A^y mice were mated with female $Atf6\alpha^{-/-}$ mice to generate $Atf6\alpha^{+/-}A^y$ mice which were further mated with female $Atf6\alpha^{-/-}$ to produce $Atf6\alpha^{-/-}A^y$ mice. Offspring positive for the A^y gene were recognized by agouti coat color. All agouti experiments were performed on the F1 generation. The mice were kept under standard, specific pathogen-free conditions with a constant dark/light cycle and free access to standard

Please cite this article as: Usui M, et al, Atf6α-null mice are glucose intolerant due to pancreatic β-cell failure on a high-fat diet but partially resistant to diet-induced..., Metabolism (2012), doi:10.1016/j.metabol.2012.01.004

mouse chow (MF; Oriental Yeast, Tokyo, Japan) and water. The high-fat diet (rodent diet with 60% energy from fat; D12492) (HFD) was purchased from Research Diets (New Brunswick, NJ, USA) and was freely accessible.

2.2. Physiological studies

Body weights (BW) were measured once every other week. Blood samples were collected from the tail vein. Intraperitoneal glucose tolerance test (IPGTT: 2 g glucose/kg BW) was started by injecting 20% glucose solution. Intraperitoneal insulin tolerance test (ITT) was performed using the regular insulin (0.75 U/kg BW for mice on normal chow and 1.5 U/kg BW for mice on an HFD). Blood glucose levels were measured by the glucose oxidase method using a Glutest glucose sensor device (Sanwa Kagaku Kenkyusho, Nagoya, Japan). Serum insulin levels were determined using an insulin ELISA kit (Morinaga Institute of Biological Science, Tokyo, Japan).

2.3. Pancreatic insulin content and hepatic triglyceride content

Mice were killed by cervical dislocation. Pancreases were removed and homogenized in acid/ethanol (0.7 mol/l HCl/ethanol 25:75) and left at −20 °C for 48 h, with sonication every 24 h. Homogenates were then centrifuged (8000*g* for 10 min) and the insulin content of the acid/ethanol supernatant fraction was measured using insulin ELISA. Frozen livers were homogenized and triglycerides were extracted with CHCl3:CH3OH (2:1, v:v), dried and resuspended in 2-propanol [28]. Triglyceride content was measured using Lipidos liquid kit (TOYOBO, Osaka, Japan).

2.4. Immunohistochemistry

Pancreases were removed and fixed in 4% formalin. Formalin-fixed paraffin-embedded sections of pancreas were deparaffinized and re-hydrated. The sections were then incubated with a guinea pig anti-insulin IgG (DAKO Japan, Kyoto, Japan) diluted 1:1000 for 1 h at room temperature.

2.5. Quantitative RT-PCR

Total RNA was isolated from 0.05 g liver with Isogen (Wako Pure Chemical, Osaka, Japan), and cDNA was synthesized with a Transcriptor First Strand cDNA Synthesis Kit (Roche Diagnostics, Mannheim, Germany) using 1 μg total RNA. Complimentary DNA synthesized from total RNA was evaluated using the real-time quantitative PCR system (Light Cycler Quick System 350S; Roche Diagnostics). The relative amounts of mRNA were calculated with β-actin mRNA as the invariant control. The primers used are described in the Supplementary Table.

2.6. Ultrastructural analysis

We performed ultrastructural analyses of pancreatic β-cells from 25-week-old mice using electron microscopy. The samples of cells were fixed with 2% glutaraldehyde plus 2% paraformaldehyde in 0.1 M phosphate buffer (PB, pH 7.4) at 4 °C, and subsequently post-fixed with 2% osmium tetroxide in 0.1 M PB at 4 °C for 2 h. Then, the specimens were dehydrated in a graded ethanol, replaced in propylene oxide, and embedded in the epoxy resin. Ultrathin sections were obtained by ultramicrotomy technique. Ultrathin sections stained with uranyl acetate at 60 °C for 20 min and modified Sato's lead solution for 5 min were submitted to transmission electron microscope observation (JEM-1200EX, JEOL). The β-cells were distinguished from α- and δ-cells by the appearance of their secretory granules. The β-cell granules had a white halo, not evident in α- and δ-cell granules.

2.7. Statistical analysis

Data are presented as means ± S.E., unless otherwise indicated. Differences between groups were assessed by Student's *t* test.

3. Results

3.1. Glucose homeostasis in ATF6α-deficient mice on normal chow

Founder *Atf6α* heterozygous knockout mice [20] were backcrossed to the C57BL/6J mice for at least 8 generations and heterozygous knockout male and female mice were mated to generate whole body *Atf6α* homo knockout mice (Fig. 1A). In the present study, we analyzed male mice, since preliminary studies showed similar phenotypes in female *Atf6α*$^{-/-}$ mice. When *Atf6α*-null mice were fed with standard chow, their body weights (BW) tended to be lower than those of wild-type (WT) mice (Fig. 1B). Blood glucose levels measured in non-fasted states were comparable between two strains (data not shown). Neither blood glucose excursions (Fig. 1C) nor insulin secretory responses (Fig. 1D) differed significantly between WT and *Atf6α*$^{-/-}$ mice when mice were subjected to an intraperitoneal glucose tolerance test (IPGTT). Insulin sensitivity, estimated by an intraperitoneal insulin (0.75 U/kg BW) tolerance test (ITT), showed that *Atf6α*$^{-/-}$ mice were somewhat more insulin sensitive, although the difference was not statistically significant (Fig. 1E). However, when ITT was performed using 2.0 U/kg BW of insulin, 5 out of 6 *Atf6α*$^{-/-}$ mice showed severe hypoglycemia of less than the lower detection limit (1.1 mM) of the glucose monitoring device at 60, and 90 min, while blood glucose levels of all WT mice were higher than 2.0 mM at 90 min (Fig. 1F), suggesting that insulin sensitivity were higher in *Atf6α*$^{-/-}$ than in WT littermates.

3.2. Glucose homeostasis in ATF6α-deficient mice fed with a high fat diet

Impaired glucose homeostasis is often associated with obesity. To further investigate roles of ATF6α in glucose homeostasis, we fed *Atf6α*$^{-/-}$ mice with a 60% high fat diet (HFD) to generate diet-induced obese (DO) animals. ATF6α-

Please cite this article as: Usui M, et al, Atf6α-null mice are glucose intolerant due to pancreatic β-cell failure on a high-fat diet but partially resistant to diet-induced..., Metabolism (2012), doi:10.1016/j.metabol.2012.01.004

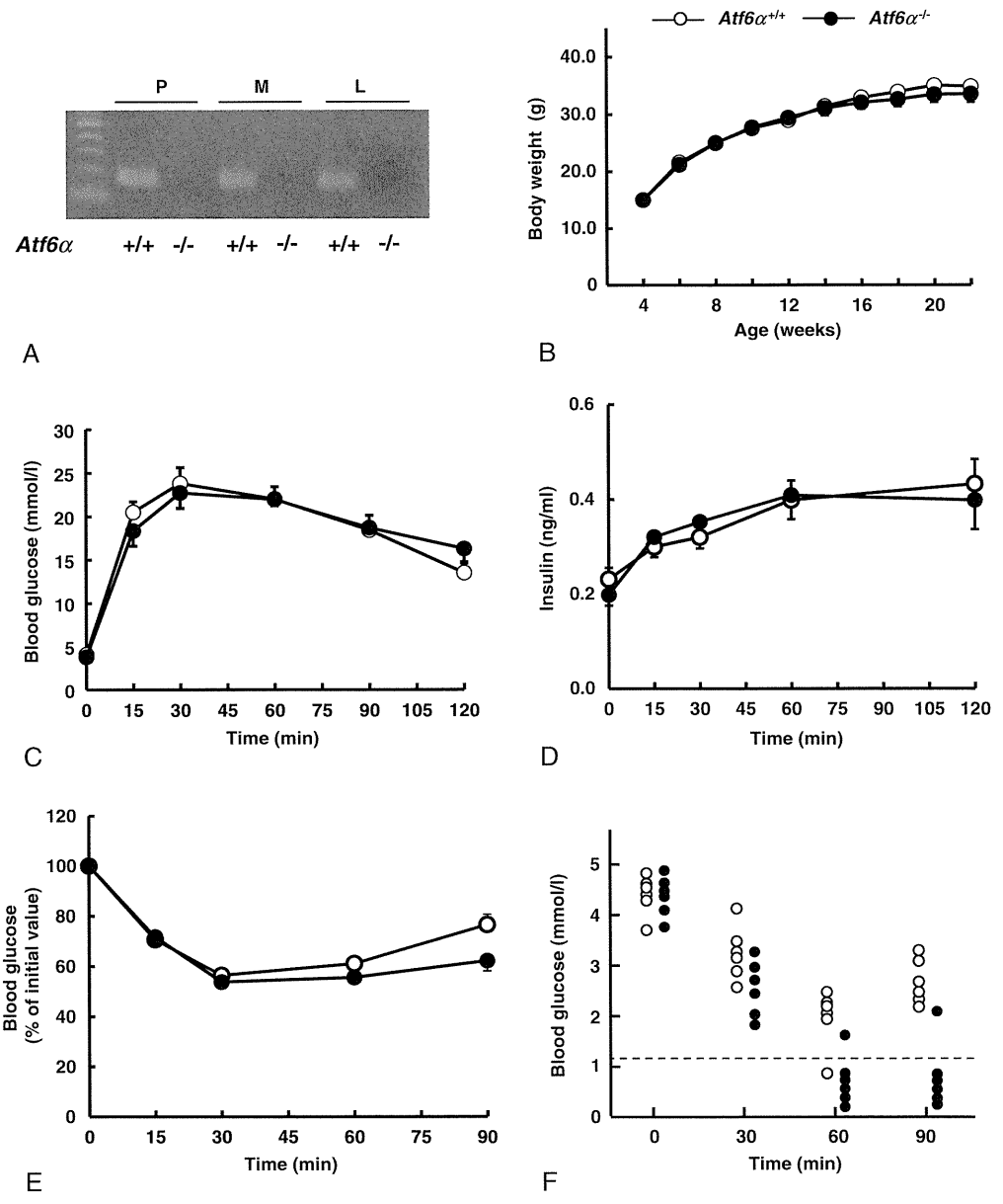

Fig. 1 – Glucose homeostasis in ATF6α-deficient mice fed with normal chow. A, Reverse transcription-PCR analysis of *Atf6α* mRNA expression in the pancreas (P), skeletal muscle (M) and liver (L) from *Atf6α*$^{+/+}$ and *Atf6α*$^{-/-}$ mice. B, Body weight of *Atf6α*$^{+/+}$ (white circles, n = 9) and *Atf6α*$^{-/-}$ (black circles, n = 13) mice. Data from three cohorts are combined. C and D, Intraperitoneal glucose tolerance tests (2 g/kg body weight) were performed at 17–19 weeks of age in *Atf6α*$^{+/+}$ (white circles, n = 9) and *Atf6α*$^{-/-}$ (black circles, n = 13) mice. Blood glucose (C) and plasma immunoreactive insulin levels (D) were measured. E, Insulin tolerance test (0.75 U/kg body weight) was performed at 21 weeks of age in *Atf6α*$^{+/+}$ (white circles, n = 7) and *Atf6α*$^{-/-}$ (black circles, n = 9) mice. F, Insulin tolerance test (2.0 U/kg body weight) was performed at 23 weeks of age in *Atf6α*$^{+/+}$ (white circles, n = 6) and *Atf6α*$^{-/-}$ (black circles, n = 6) mice. In one *Atf6α*$^{+/+}$ mouse at 60 min and 5 *Atf6α*$^{-/-}$ mice at 60 and 90 min, blood glucose levels were below the detection limit (1.1 mM, dashed line).

deficient DO mice tended to gain less weight (Fig. 2A) and showed similar blood glucose levels to those of WT-DO mice at non-fasted states (Fig. 2B). An IPGTT exhibited that ATF6α-deficient DO mice were less glucose tolerant (Fig. 2C) with reduced insulin secretion (Fig. 2D). On an HFD, it was evident that ATF6α-deficient mice were more insulin sensitive (Fig. 2E). We also measured serum lipid content in these mice. As shown in Fig. 2F, an HFD-induced increase in the serum triglyceride (TG) concentration was partially suppressed in *Atf6α*$^{-/-}$DO mice.

3.3. *Pancreatic β-cells suffered from ER stress in ATF6α-deficient mice fed with a high fat diet*

Although serum insulin levels in *Atf6α*$^{-/-}$DO mice (Fig. 2D) were lower than those in WT-DO mice, they were 3 times

Please cite this article as: Usui M, et al, Atf6α-null mice are glucose intolerant due to pancreatic β-cell failure on a high-fat diet but partially resistant to diet-induced..., Metabolism (2012), doi:10.1016/j.metabol.2012.01.004

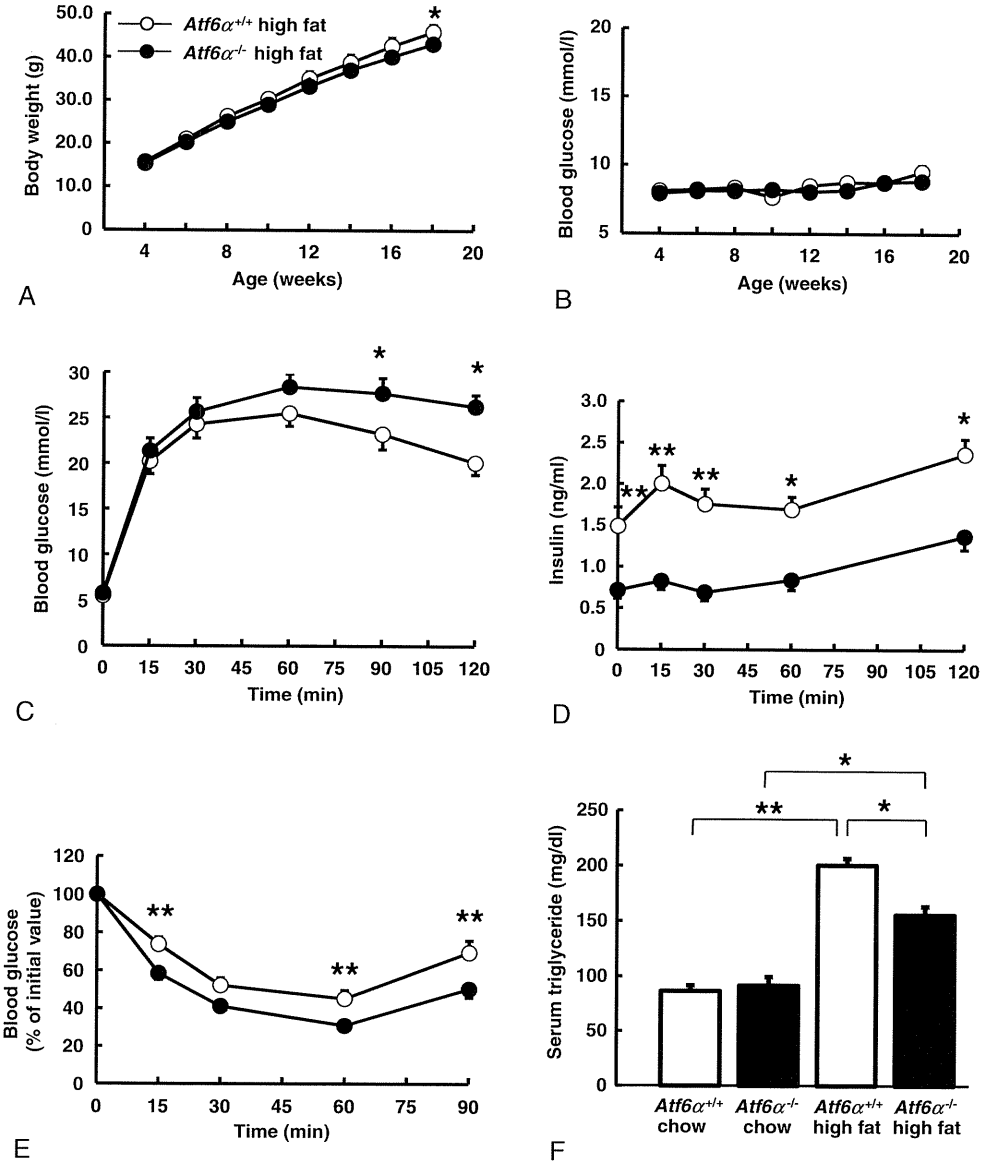

Fig. 2 – Metabolic homeostasis in ATF6α-deficient mice fed with an HFD. A and B, Body weight (A) and non-fasted glucose (B) were measured in *Atf6α*$^{+/+}$ (white circles, *n* = 12) and *Atf6α*$^{-/-}$ (black circles, *n* = 17) mice fed with an HFD. *P < .05. C and D, Intraperitoneal glucose tolerance test (1.5 g/kg body weight) was performed at 17–19 weeks of age in *Atf6α*$^{+/+}$ (white circles, *n* = 12) and *Atf6α*$^{-/-}$ (black circles, *n* = 17) mice on an HFD. Blood glucose (C) and plasma immunoreactive insulin levels (D) were measured. *P < .05, **P < .01. E, Insulin tolerance test (1.5 U/kg) was performed at 20–22 weeks of age in *Atf6α*$^{+/+}$ (white circles, *n* = 12) and *Atf6α*$^{-/-}$ (black circles, *n* = 17) mice on an HFD. **P < .01. F, Serum triglyceride levels were measured at the 17–19 weeks of age in *Atf6α*$^{+/+}$ (*n* = 8) and *Atf6α*$^{-/-}$ (*n* = 7) mice on normal chow as well as *Atf6α*$^{+/+}$ (*n* = 11) and *Atf6α*$^{-/-}$ (*n* = 13) mice on an HFD. *P < .05, **P < .01.

higher than those in ATF6α-deficient mice fed with normal chow (Fig. 1D). The homeostasis model assessment of insulin resistance index was 2.20, 1.66, 9.81 and 4.58, for WT on normal chow, *Atf6α*$^{-/-}$ on normal chow, WT on an HFD and *Atf6α*$^{-/-}$ on an HFD, respectively. These results indicated that *Atf6α*$^{-/-}$DO mice developed insulin resistance, although milder than WT mice. Therefore, it was reasonable to speculate that lower insulin secretion in *Atf6α*$^{-/-}$DO mice could result from β-cell failure in adaptation to increased insulin resistance. In order to gain insight into β-cell homeostasis in *Atf6α*$^{-/-}$DO mice, pancreatic insulin content was measured. While pancreatic insulin content increased upon HFD feeding in WT mice, *Atf6α*$^{-/-}$ mice did not respond to the HFD by increasing insulin production (Fig. 3A). We then analyzed ultrastructure of β-cells in *Atf6α*$^{-/-}$ mice fed with an HFD. As indicated in Fig. 3B, while the ER in β-cells showed compact reticulate structure in WT-DO mice, in *Atf6α*$^{-/-}$DO mouse β-cells, frequently observed was swollen ER, a typical phenotype of ER stressed cells [29]. These data indicate that ATF6α-deficient β-cells suffered from ER stress due to increased demands of insulin production, and suggest that lower insulin secretion was, at least partly, caused by ER

Please cite this article as: Usui M, et al, Atf6α-null mice are glucose intolerant due to pancreatic β-cell failure on a high-fat diet but partially resistant to diet-induced..., Metabolism (2012), doi:10.1016/j.metabol.2012.01.004

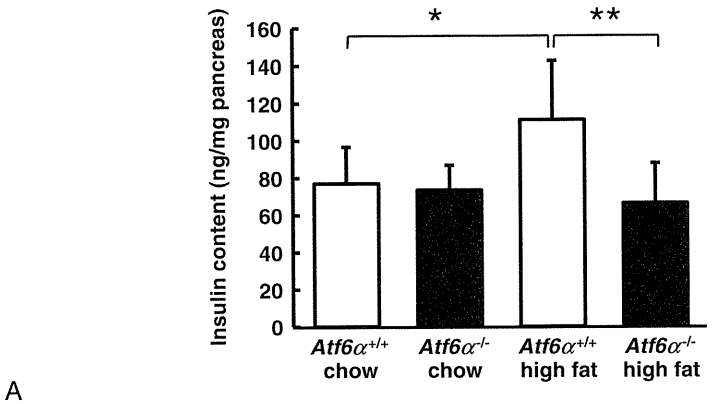

A

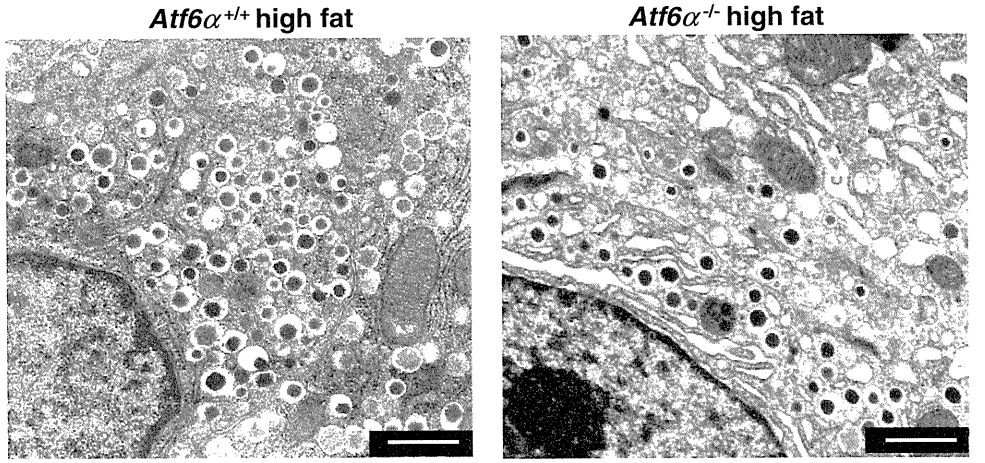

B

Fig. 3 – Pancreatic β-cell homeostasis in *Atf6α*$^{-/-}$ mice on an HFD. A, Pancreatic insulin content was measured in *Atf6α*$^{+/+}$ (n = 6) and *Atf6α*$^{-/-}$ (n = 5) mice on normal chow as well as *Atf6α*$^{+/+}$ (n = 10) and *Atf6α*$^{-/-}$ (n = 13) mice on an HFD at 25 weeks of age. *P < .05, **P < .01. B, Ultrastructural analysis was performed on islets of *Atf6α*$^{+/+}$ (n = 3) and *Atf6α*$^{-/-}$ (n = 3) mice on HFD at 25 weeks of age. Representative micrographs of β-cells are shown. Bars, 1 μm.

stress-induced failure in maintaining insulin content in ATF6α-deficient pancreas.

3.4. *Impact of ATF6 deficiency on liver homeostasis in mice fed with a high fat diet*

It is known that ER stress is increased in the liver of HFD-fed mice [7]. Thus, we analyzed effects of ATF6α deficiency on UPR gene expressions in the liver. XBP-1 mRNA splicing was augmented (Fig. 4A) and ATF4 mRNA levels was increased (Fig. 4B) in livers of *Atf6α*$^{-/-}$DO mice, indicating that higher ER stress existed when the ATF6α-deficient liver was metabolically overloaded. Since recent studies have indicated the involvement of UPR mediators in hepatic lipogenesis or glycolysis [30,31], we measured expressions of lipogenic or glycolytic enzymes. We found that mRNA expressions of a gluconeogenic enzyme glucose-6-phosphatase (G6P) and those of PPAR-γ and SREBP1c, master regulators of lipogenic enzymes, were increased in ATF6α-deficient DO mice (Fig. 4B). These findings have prompted us to measure liver TG content and to conduct morphological analysis of the liver in these animals. Liver TG content tended to increase in *Atf6α*$^{-/-}$DO mice although the difference failed to reach statistical significance (P = .069, Fig. 4C). Liver sections showed increased lipid droplets in *Atf6α*$^{-/-}$DO mice (Fig. 4D), suggesting that steatosis was enhanced with ATF6α deficiency.

3.5. *ATF6α deficiency in Agouti yellow obese mice, a genetic diabetes model with increased insulin resistance*

To confirm effects of ATF6α deficiency on insulin resistance, ATF6α-deficient mice were crossed with Agouti yellow (A^y) mice. A^y mice develop obesity and insulin resistance because of blockade of hypothalamic melanocortin-4 receptors due to ectopic expression of agouti peptide and thus are resistant to the satiety [32,33]. The phenotypes of *Atf6α*$^{-/-}$$A^y$ mice were similar to those of *Atf6α*$^{-/-}$DO mice. Body weights of *Atf6α*$^{-/-}$$A^y$ mice were significantly lower than those of A^y mice (Fig. 5A). Although blood glucose levels were similar between the two strains (Fig. 5B), glucose excursion after an intraperitoneal glucose challenge was greater with reduced insulin secretion in *Atf6α*$^{-/-}$$A^y$ mice (Figs. 5C and 5D). Insulin sensitivity estimated by ITT was also higher in ATF6α-deficient A^y mice (Fig. 5E). Pancreatic insulin content was approximately 50% lower in *Atf6α*$^{-/-}$$A^y$ mice than in WT mice at 25 weeks of age (Fig. 5F).

Please cite this article as: Usui M, et al, Atf6α-null mice are glucose intolerant due to pancreatic β-cell failure on a high-fat diet but partially resistant to diet-induced..., Metabolism (2012), doi:10.1016/j.metabol.2012.01.004

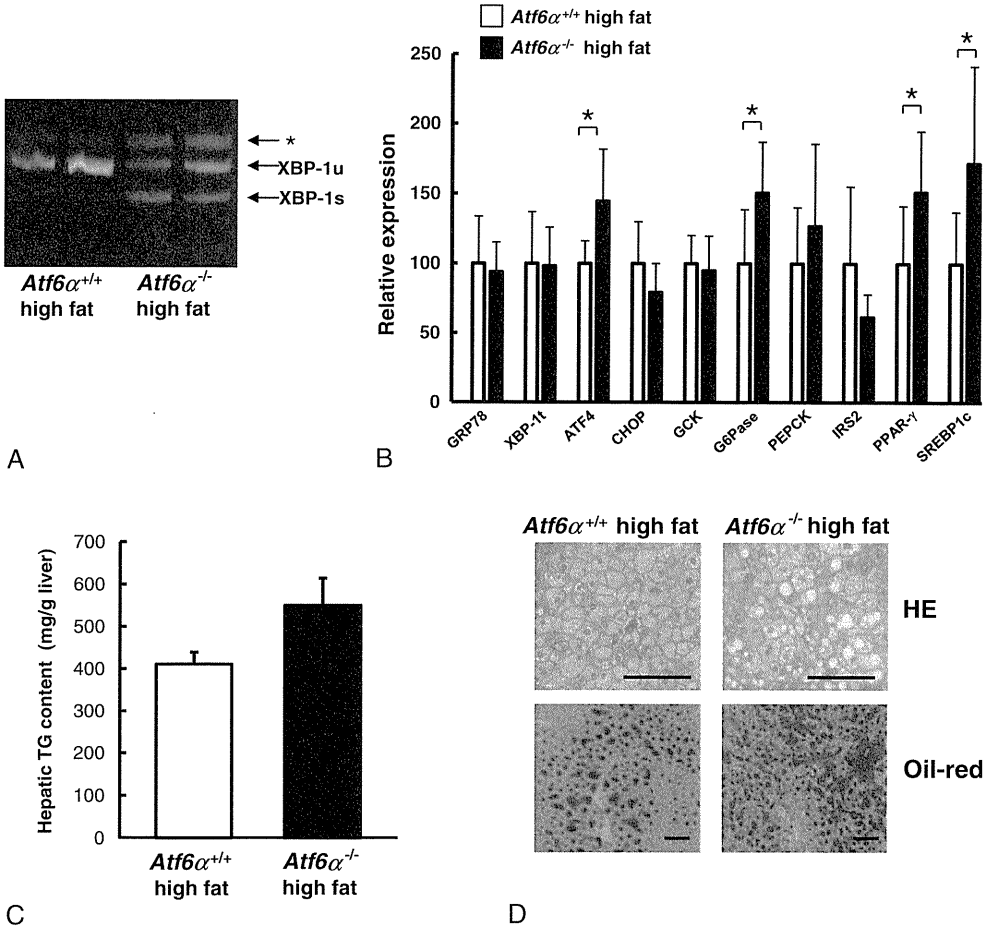

Fig. 4 – Impact of ATF6 deficiency on liver homeostasis in mice on an HFD. A, Spliced (XBP-1s) and unspliced (XBP-1u) forms of XBP-1 mRNA were analyzed in liver of WT and *Atf6α*$^{-/-}$ mice on an HFD. The data are representative of 5 experiments. *Non-specific band. B, Quantitative RT-PCR was conducted using total RNA extracted from *Atf6α*$^{+/+}$ (n = 6) and *Atf6α*$^{-/-}$ (n = 11) mouse liver on an HFD at 25 weeks of age. XBP-1t: total XBP-1 mRNA. Data are presented as β-actin corrected value ± SD. *$P < .05$. C, TG content of liver was measured using liver homogenates from *Atf6α*$^{+/+}$ (white bars, n = 7) and *Atf6α*$^{-/-}$ (black bars, n = 9) mice on an HFD at 21 weeks of age. D, *Atf6α*$^{+/+}$ and *Atf6α*$^{-/-}$ mouse liver sections were stained with hematoxylin–eosin and oil-red O at 25 weeks of age. Bars, 100 μm.

3.6. *ATF6α deficiency in Ins2*$^{WT/C96Y}$ *mice, a genetic diabetes model with ER-stress induced β-cell failure*

Studies on pancreas of *Atf6α*$^{-/-}$DO mice showed that ATF6-deficient β-cells suffered from ER stress. Thus, roles of ATF6α in β-cells under ER stress were also studied in *Atf6α*$^{-/-}$ mice bred with *Ins2*$^{WT/C96Y}$ (Akita) mice. In the latter mutant mice, insulin molecule with a Cys96Tyr mutation cannot fold correctly and causes ER stress in β-cells, leading to β-cell death and diabetes [27]. Reduction in BW and exaggerated hyperglycemia were evident in *Atf6α*$^{-/-}$*Ins2*$^{WT/C96Y}$ mice compared with *Atf6α*$^{+/+}$*Ins2*$^{WT/C96Y}$ mice (Figs. 6A and 6B). Pancreas insulin content from *Atf6α*$^{-/-}$*Ins2*$^{WT/C96Y}$ mice was 50% of that from *Atf6α*$^{+/+}$ *Ins2*$^{WT/C96Y}$ mice at 4–5 weeks of age, which was already reduced to one-third that from WT pancreas (Fig. 6C), with the majority of islets being smaller than those in *Ins2*$^{WT/C96Y}$ mice (Fig. 6D). These data showed that ATF6α contributes to the protection of β-cells against ER stress caused by mutated insulin Cys96Tyr in vivo.

4. Discussion

ATF6α, an ER stress sensor molecule, plays a critical role in initiation and development of the UPR. Recent studies indicated that ER stress itself and/or the UPR signaling are implicated in several components of the diabetes pathophysiology, including reduced β-cell mass, increased insulin resistance, ectopic lipid accumulation and hyperlipidemia. Thus, it has been speculated that ATF6α deficiency would have an impact on metabolic homeostasis. Our analysis of ATF6α-deficient mice revealed that ATF6α contributes to both prevention and promotion of the metabolic disorder in vivo.

In the absence of environmental challenges, *Atf6α*$^{-/-}$ mice maintained normal glucose homeostasis with normal insulin secretory responses, indicating that β-cells without ATF6α have the capacity to deal with the large amount of proinsulin under the physiological condition. However, when metabolic overload further demanded to produce and secrete greater

Please cite this article as: Usui M, et al, Atf6α-null mice are glucose intolerant due to pancreatic β-cell failure on a high-fat diet but partially resistant to diet-induced..., Metabolism (2012), doi:10.1016/j.metabol.2012.01.004

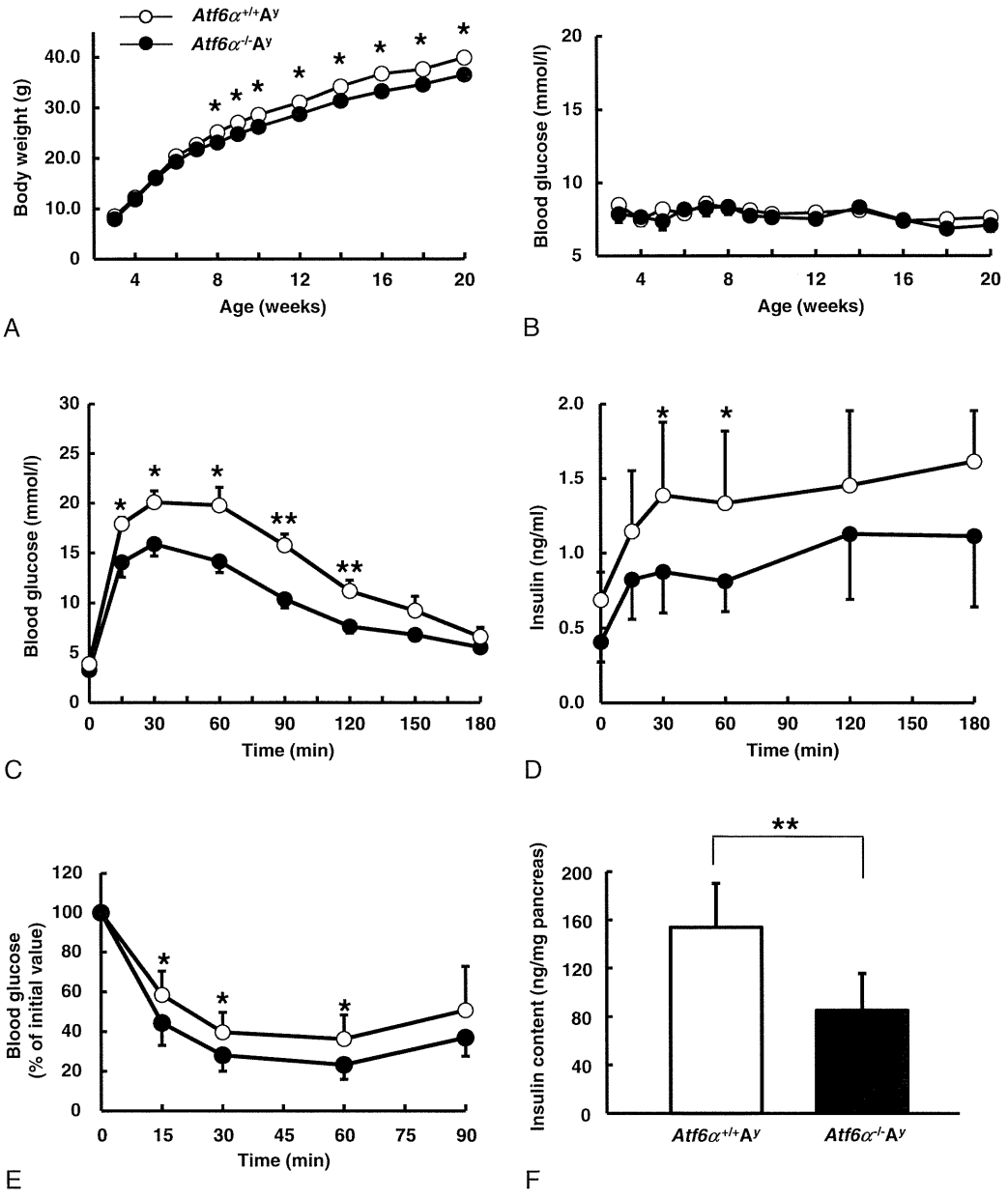

Fig. 5 – Glucose homeostasis in ATF6α-deficient A^y mice. A and B, Body weight (A) and glucose levels (B) on fed conditions were measured in *Atf6*$\alpha^{+/+}A^y$ (white circles, $n = 10$) and *Atf6*$\alpha^{-/-}A^y$ (black circles, $n = 13$) mice. Data from four cohorts are combined. *P < .05. C and D, Intraperitoneal glucose tolerance tests (1.5 g/kg body weight) were performed at 17–19 weeks of age in *Atf6*$\alpha^{+/+}A^y$ (white circles, $n = 7$) and *Atf6*$\alpha^{-/-}A^y$ (black circles, $n = 8$) mice. Blood glucose (C) and plasma immunoreactive insulin levels (D) were measured. *P < .05, **P < .01. E, Insulin tolerance tests (1.5 U/kg) were performed (E) at 20–22 weeks of age in *Atf6*$\alpha^{+/+}A^y$ (white circles, $n = 7$) and *Atf6*$\alpha^{-/-}A^y$ (black circles, $n = 8$) mice. *P < .05. F: Pancreatic insulin content was measured in *Atf6*$\alpha^{+/+}A^y$ ($n = 6$) and *Atf6*$\alpha^{-/-}A^y$ ($n = 8$) mice at 25 weeks of age. **P < .01.

amount of insulin, the ATF6α-deficient β-cell failed to cope with the stress. Thus, we observed swollen ER, a typical phenotype of the stressed ER [29], in the β-cell of *Atf6*$\alpha^{-/-}$DO mice. The β-cell failure under the HFD seemed to be also caused by increased circulating lipid levels, as lipotoxicity is also a cause of ER stress [34]. We did not examine β-cell mass in *Atf6*$\alpha^{-/-}$DO mice. Therefore, it was not clear that lower pancreatic insulin content in *Atf6*$\alpha^{-/-}$DO mice resulted either from reduced insulin production in individual β-cells or from reduction in β-cell mass. Nonetheless, we prefer the latter possibility, since islets became smaller when the *Atf6*α gene was deleted in β-cells with misfolded insulin molecules in Akita *Ins2*$^{WT/C96Y}$ mice. These data suggest that ATF6α plays an important role in β-cell survival under ER stress conditions.

It has been known that ER stress plays a role in metabolic regulation in the liver. ATF6α reportedly suppresses gluconeogenesis by inhibiting transcription of gluconeogenic enzymes [35,36]. In accordance with this notion, we observed increased G6P expression, possibly contributing to impaired glucose homeostasis in ATF6α-deficient DO mice.

Please cite this article as: Usui M, et al, Atf6α-null mice are glucose intolerant due to pancreatic β-cell failure on a high-fat diet but partially resistant to diet-induced..., Metabolism (2012), doi:10.1016/j.metabol.2012.01.004

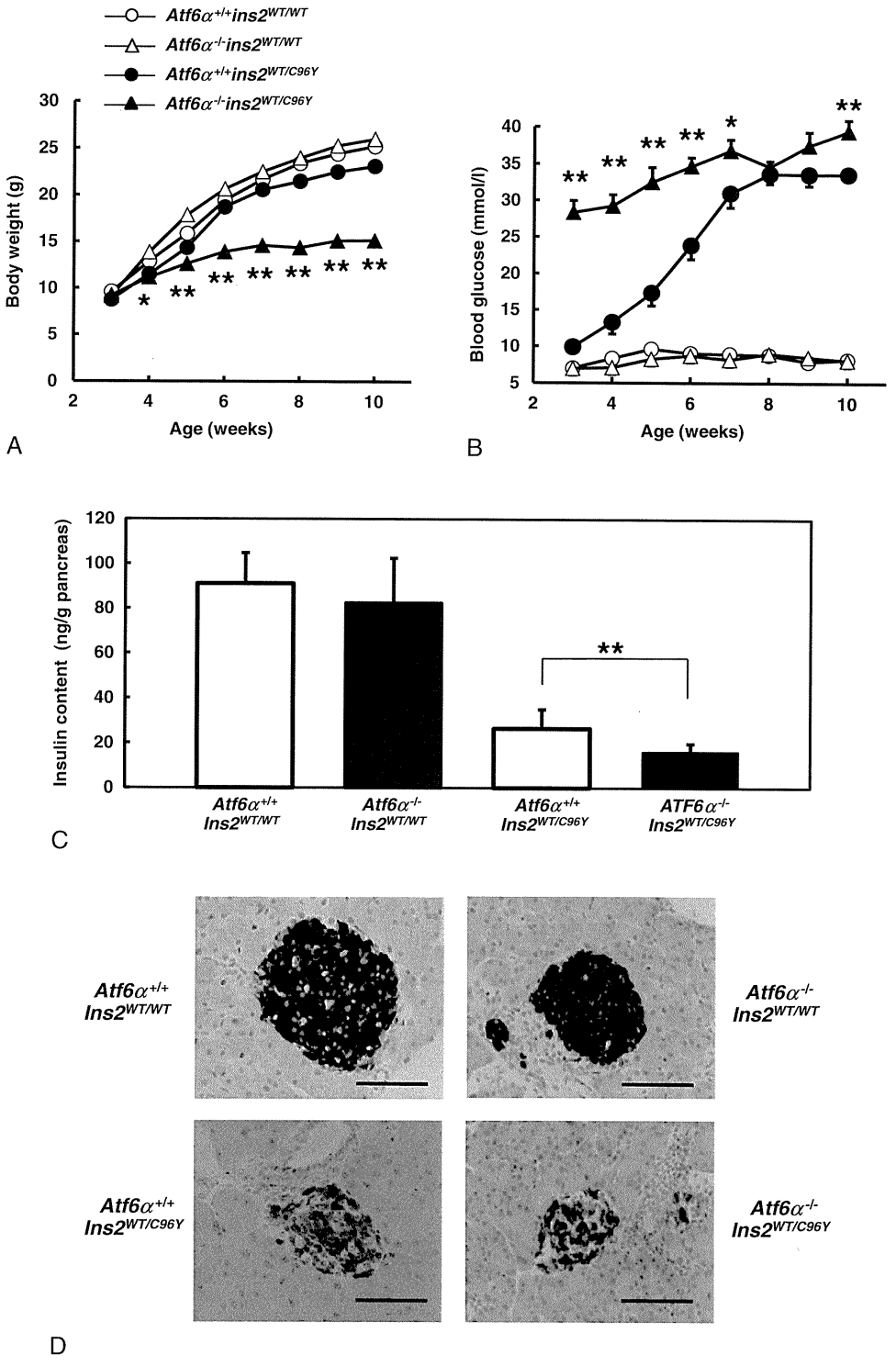

Fig. 6 – ATF6α deficiency exaggerated hyperglycemia in $Ins2^{WT/C96Y}$ mice. A and B, Body weight (A) and glucose levels (B) on fed conditions were measured in $Atf6\alpha^{+/+}$ (white circles, n = 12), $Atf6\alpha^{+/+}Ins2^{WT/C96Y}$ (black circles, n = 16), $Atf6\alpha^{-/-}$ (white triangles, n = 13) and $Atf6\alpha^{-/-}Ins2^{WT/C96Y}$ (black triangles, n = 15) mice. *P < .05, **P < .01 compared with the $Atf6\alpha^{+/+}Ins2^{WT/C96Y}$ mice. C, Pancreatic insulin content of $Atf6\alpha^{+/+}$ (n = 8), $Atf6\alpha^{-/-}$(n = 9), $Atf6\alpha^{+/+}Ins2^{WT/C96Y}$ (n = 11) and $Atf6\alpha^{-/-}Ins2^{WT/C96Y}$ (n = 11) mice at 4–5 weeks of age. **P < .01. D, Pancreas section of mice with indicated genotypes at 4–5 weeks of age was immunostained for insulin. Bars, 100 μm.

Recent studies have also revealed a link between ER stress and hepatic steatosis. $Atf6\alpha^{-/-}$ mice [19,37], mice with liver-specific deletion of functional eIF2α [19], and liver-specific IRE1α knockout mice [19], all developed hepatic steatosis when a pharmacological ER stress inducer, tunicamycin (a protein glycosylation inhibitor) was injected. Here, we

Please cite this article as: Usui M, et al, Atf6α-null mice are glucose intolerant due to pancreatic β-cell failure on a high-fat diet but partially resistant to diet-induced..., Metabolism (2012), doi:10.1016/j.metabol.2012.01.004

demonstrated that greater levels of ER stress were present with increased tendency to develop a higher degree of hepatosteatosis in liver of ATF6α-deficient DO mice. Thus, our data indicate that not only acute pharmacological ER stress but also chronic ER stress promoted the development of hepatosteatosis. It has been postulated that ER stress-mediated activation of metabolic master regulator proteins, such as PPAR-γ and SREBP1c, contributes to liver steatosis [19,30]. A direct role of ATF6α in regulation of lipid homeostasis has been also postulated: ATF6α attenuates lipogenesis in the liver by suppressing SERBP2 [38]. Interestingly, we observed that despite increased lipid accumulation in the liver, circulating triglyceride levels were lower in *Atf6α*$^{-/-}$DO mice. These data suggest defects in impaired very low-density lipoprotein (VLDL) formation or triglyceride transfer to the circulation. A recent article indicated that ER stress-mediated reduction in stability of apolipoprotein B-100, a major protein component of VLDL, caused lipid accumulation in the liver of *Atf6α*$^{-/-}$ mice injected with tunicamycin [37]. A similar mechanism might be involved in the liver of *Atf6α*$^{-/-}$DO mice under chronic ER stress, which leads to liver steatosis.

An interesting observation made in this study was that ATF6α deficiency resulted in improved insulin sensitivity. *Atf6α*-null mice were partially resistant to development of insulin resistance resulting from metabolic overload induced by two different manners: placing on a high fat diet or introducing the agouti mutation causing hyperphagia. The mechanism by which ATF6α deficiency made mice partially resistant to the development of insulin resistance is currently unknown. It has been shown that the serum triglyceride level is a factor of insulin resistance [39,40]. Therefore, partial suppression in the development of hypertriglyceridemia might cause improved insulin sensitivity in ATF6α-deficient DO mice.

The present data indicate that ATF6α protects pancreatic β-cells from ER stress-induced cell damage. It also seems to protect liver tissue from steatosis under the HFD, but contributes to development of hyperlipidemia and insulin resistance in mice. Thus, ATF6α affects whole body glucose homeostasis through tissue specific actions. A limitation of the present study, in which whole body knockout mice were analyzed, is that some phenotypes of one tissue could be influenced by those of other tissues with ATF6α deficiency. Future studies using tissue specific ATF6α knockout mice would clarify these issues.

Supplementary materials related to this article can be found online at doi:10.1016/j.metabol.2012.01.004.

Funding

This research was supported by a Grant-in-Aid for Scientific Research (H16-genome-003) to Y.O. from the Ministry of Health, Labor and Welfare of Japan. This work was also supported by the 21st Global COE Program to Y.O. and a Grant-in-Aid for Scientific Research (21591147) to H.I. from the Ministry of Education, Science, Sports and Culture of Japan and a research grant from the Takeda Science Foundation to H.I.

Acknowledgment

We are grateful to C. Suzuki and M. Kato for their expert technical assistance.

REFERENCES

[1] Kasuga M. Insulin resistance and pancreatic β cell failure. J Clin Invest 2006;116:1756-60.
[2] Sakuraba H, Mizukami H, Yagihashi N, et al. Reduced β-cell mass and expression of oxidative stress-related DNA damage in the islet of Japanese type II diabetic patients. Diabetologia 2002;45:85-96.
[3] Butler AE, Janson J, Soeller WC, et al. Increased β-cell apoptosis prevents adaptive increase in β-cell mass in mouse model of type 2 diabetes: evidence for role of islet amyloid formation rather than direct action of amyloid. Diabetes 2003;52:2304-14.
[4] Rahier J, Guiot Y, Goebbels RM, et al. Pancreatic β-cell mass in European subjects with type 2 diabetes. Diabetes Obes Metab 2008;10(Suppl 4):32-42.
[5] Eizirik DL, Cardozo AK, Cnop M. The role for endoplasmic reticulum stress in diabetes mellitus. Endocr Rev 2008;29: 42-61.
[6] Scheuner D, Kaufman RJ. The unfolded protein response: a pathway that links insulin demand with β-cell failure and diabetes. Endocr Rev 2008;29:317-33.
[7] Ozcan U, Cao Q, Yilmaz E, et al. Endoplasmic reticulum stress links obesity, insulin action, and type 2 diabetes. Science 2004;306:457-61.
[8] Hotamisligil GS. Endoplasmic reticulumn stress and the inflamatory basis of metabolic disease. Cell 2010;140:900-17.
[9] Boden G, Duan X, Homko C, et al. Increase in endoplasmic reticulum stress-related proteins and genes in adipose tissue of obese, insulin-resistant individuals. Diabetes 2008;57: 2438-44.
[10] Gregor MF, Yang L, Fabbrini E, et al. Endoplasmic reticulum stress is reduced in tissues of obese subjects after weight loss. Diabetes 2009;58:693-700.
[11] Sharma NK, Das SK, Mondal AK, et al. Endoplasmic reticulum stress markers are associated with obesity in nondiabetic subjects. J Clin Endocrinol Metab 2008;93:4532-41.
[12] Ron D, Walter P. Signal integration in the endoplasmic reticulum unfolded protein response. Nat Rev Mol Cell Biol 2007;8:519-29.
[13] Oslowski CM, Urano F. A switch from life to death in endoplasmic reticulum stressed β-cells. Diabetes Obes Metab 2010;12(Suppl 2):58-65.
[14] Harding HP, Zhang Y, Ron D. Protein translation and folding are coupled by an endoplasmic-reticulum-resident kinase. Nature 1999;397:271-4.
[15] Harding HP, Zeng H, Zhang Y, et al. Diabetes mellitus and exocrine pancreatic dysfunction in perk–/– mice reveals a role for translational control in secretory cell survival. Mol Cell 2001;7:1153-63.
[16] Urano F, Wang X, Bertolotti A, et al. Coupling of stress in the ER to activation of JNK protein kinases by transmembrane protein kinase IRE1. Science 2000;287:664-6.
[17] Delepine M, Nicolino M, Barrett T, et al. EIF2AK3, encoding translation initiation factor 2-α kinase 3, is mutated in patients with Wolcott-Rallison syndrome. Nat Genet 2000;25: 406-9.
[18] Rutkowski DT, Wu J, Back SH, et al. UPR pathways combine to prevent hepatic steatosis caused by ER stress-mediated suppression of transcriptional master regulators. Dev Cell 2008;15:829-40.

Please cite this article as: Usui M, et al, Atf6α-null mice are glucose intolerant due to pancreatic β-cell failure on a high-fat diet but partially resistant to diet-induced..., Metabolism (2012), doi:10.1016/j.metabol.2012.01.004

[19] Wu J, Rutkowski DT, Dubois M, et al. ATF6α optimizes long-term endoplasmic reticulum function to protect cells from chronic stress. Dev Cell 2007;13:351-64.
[20] Yamamoto K, Sato T, Matsui T, et al. Transcriptional induction of mammalian ER quality control proteins is mediated by single or combined action of ATF6α and XBP1. Dev Cell 2007;13:365-76.
[21] Laybutt DR, Preston AM, Akerfeldt MC, et al. Endoplasmic reticulum stress contributes to β cell apoptosis in type 2 diabetes. Diabetologia 2007;50:752-63.
[22] Meex SJ, Weissglas-Volkov D, van der Kallen CJ, et al. The ATF6-Met[67]Val substitution is associated with increased plasma cholesterol levels. Arterioscler Thromb Vasc Biol 2009;29:1322-7.
[23] Chu WS, Das SK, Wang H, et al. Activating transcription factor 6 (ATF6) sequence polymorphisms in type 2 diabetes and pre-diabetic traits. Diabetes 2007;56:856-62.
[24] Meex SJ, van Greevenbroek MM, Ayoubi TA, et al. Activating transcription factor 6 polymorphisms and haplotypes are associated with impaired glucose homeostasis and type 2 diabetes in Dutch Caucasians. J Clin Endocrinol Metab 2007;92:2720-5.
[25] Thameem F, Farook VS, Bogardus C, et al. Association of amino acid variants in the activating transcription factor 6 gene (ATF6) on 1q21-q23 with type 2 diabetes in Pima Indians. Diabetes 2006;55:839-42.
[26] Hu C, Zhang R, Wang C, et al. Lack of association between genetic polymorphisms within DUSP12 - ATF6 locus and glucose metabolism related traits in a Chinese population. BMC Med Genet 2011;12:3.
[27] Wang J, Takeuchi T, Tanaka S, et al. A mutation in the insulin 2 gene induces diabetes with severe pancreatic β-cell dysfunction in the Mody mouse. J Clin Invest 1999;103:27-37.
[28] Folch J, Lees M, Sloane Stanley GH. A simple method for the isolation and purification of total lipides from animal tissues. J Biol Chem 1957;226:497-509.
[29] Scheuner D, van der Mierde D, Song B, et al. Control of mRNA translation preserves endoplasmic reticulum function in β cells and maintains glucose homeostasis. Nat Med 2005;11: 757-64.
[30] Kammoun HL, Chabanon H, Hainault I, et al. GRP78 expression inhibits insulin and ER stress-induced SREBP-1c activation and reduces hepatic steatosis in mice. J Clin Invest 2009;119:1201-15.
[31] Liu J, Jin X, Yu CH, et al. Endoplasmic reticulum stress involved in the course of lipogenesis in fatty acids-induced hepatic steatosis. J Gastroenterol Hepatol 2010;25:613-8.
[32] Fan W, Boston BA, Kesterson RA, et al. Role of melanocortinergic neurons in feeding and the agouti obesity syndrome. Nature 1997;385:165-8.
[33] Huszar D, Lynch CA, Fairchild-Huntress V, et al. Targeted disruption of the melanocortin-4 receptor results in obesity in mice. Cell 1997;88:131-41.
[34] Cnop M, Ladrière L, Igoillo-Esteve M, et al. Causes and cures for endoplasmic reticulum stress in lipotoxic β-cell dysfunction. Diabetes Obes Metab 2010;12(Suppl 2):76-82.
[35] Seo HY, Kim MK, Min AK, et al. Endoplasmic reticulum stress-induced activation of activating transcription factor 6 decreases cAMP-stimulated hepatic gluconeogenesis via inhibition of CREB. Endocrinology 2010;151:561-8.
[36] Wang Y, Vera L, Fischer WH, et al. The CREB coactivator CRTC2 links hepatic ER stress and fasting gluconeogenesis. Nature 2009;460:534-7.
[37] Yamamoto K, Takahara K, Oyadomari S, et al. Induction of liver steatosis and lipid droplet formation in ATF6α-knockout mice burdened with pharmacological endoplasmic reticulum stress. Mol Biol Cell 2010;21:2975-86.
[38] Zeng L, Lu M, Mori K, et al. ATF6 modulates SREBP2-mediated lipogenesis. EMBO J 2004;23:950-8.
[39] Taniguchi A, Nakai Y, Sakai M, et al. Relationship of regional adiposity to insulin resistance and serum triglyceride levels in nonobese Japanese type 2 diabetes patioents. Metabolism 2002;51:544-8.
[40] Hollander WL, Bikman BT, Wang LP, et al. Lipid-induced insulin resistance mediated by the proinflammatory receptor TLR4 requires saturated fatty acid-induced ceramide biosynthesis in mice. J Clin Invest 2011;121:1858-70.

Please cite this article as: Usui M, et al, Atf6α-null mice are glucose intolerant due to pancreatic β-cell failure on a high-fat diet but partially resistant to diet-induced..., Metabolism (2012), doi:10.1016/j.metabol.2012.01.004

Open

Hypertension Research (2012) 35, 213–220

www.nature.com/hr

ORIGINAL ARTICLE

Modulation of renal superoxide dismutase by telmisartan therapy in C57BL/6-*Ins2*^{Akita} diabetic mice

Hiroki Fujita[1], Hiromi Fujishima[1], Tsukasa Morii[1], Takuya Sakamoto[2], Koga Komatsu[2], Mihoko Hosoba[1], Takuma Narita[1], Keiko Takahashi[3], Takamune Takahashi[3] and Yuichiro Yamada[1]

Renal superoxide excess, which is induced by an imbalance of the superoxide-producing enzyme NAD(P)H oxidase and the superoxide-scavenging enzyme superoxide dismutase (SOD) under hyperglycemia, increases oxidative stress and contributes to the development of diabetic nephropathy. In this study, we treated non-obese and hypoinsulinemic C57BL/6-*Ins2*^{Akita} (C57BL/6-Akita) diabetic mice with telmisartan (5 mg kg^{-1} per day), an angiotensin II type 1 receptor blocker, or amlodipine (5 mg kg^{-1} per day), a calcium channel blocker, for 4 weeks and compared the effects of these two anti-hypertensive drugs on renal NAD(P)H oxidase, SOD and transcription factor Nrf2 (NF-E2-related factor 2), which is known to upregulate several antioxidant enzymes including SOD. Vehicle-treated C57BL/6-Akita mice exhibited higher renal NAD(P)H oxidase and lower renal SOD activity with increased levels of renal superoxide than the C57BL/6-wild-type non-diabetic mice. Interestingly, telmisartan treatment not only reduced NAD(P)H oxidase activity but also enhanced SOD activity in C57BL/6-Akita mouse kidneys, leading to a reduction of renal superoxide levels. Furthermore, telmisartan-treated C57BL/6-Akita mice increased the renal protein expression of SOD and Nrf2. In parallel with the reduction of renal superoxide levels, a reduction of urinary albumin levels and a normalization of elevated glomerular filtration rate were observed in telmisartan-treated C57BL/6-Akita mice. In contrast, treatment with amlodipine failed to modulate renal NAD(P)H oxidase, SOD and Nrf2. Finally, treatment of C57BL/6-Akita mice with apocynin, an NAD(P)H oxidase inhibitor, also increased the renal protein expression of SOD and Nrf2. Collectively, our data suggest that NAD(P)H oxidase negatively regulates renal SOD, possibly by downregulation of Nrf2, and that telmisartan could upregulate renal SOD by the suppression of NAD(P)H oxidase and subsequent upregulation of Nrf2, leading to the amelioration of renal oxidative stress and diabetic renal changes.
Hypertension Research (2012) **35,** 213–220; doi:10.1038/hr.2011.176; published online 10 November 2011

Keywords: angiotensin II type 1 receptor blocker; diabetic nephropathy; NAD(P)H oxidase; superoxide dismutase; telmisartan

INTRODUCTION

Growing evidence indicates that superoxide anion ($O_2^{\bullet -}$) excess induced by chronic hyperglycemia contributes to glomerular injury, which characterizes diabetic nephropathy (DN) through the formation of secondary reactive oxygen species including peroxynitrite and hydroxyl radicals.[1–4] Two endogenous enzymes, NAD(P)H oxidase and superoxide dismutase (SOD), are thought to be key determinants for the superoxide anion levels in kidneys. NAD(P)H oxidase is the most important source of superoxide anions,[5–8] whereas SOD is a major defender against superoxide anions.[9,10] SOD consists of three enzymatic isoforms: cytosolic CuZn-SOD (SOD1), mitochondrial Mn-SOD (SOD2), and extracellular CuZn-SOD (SOD3).[10,11] These three isoforms are derived from distinct genes but catalyze the same reaction.[11] Each SOD isoform neutralizes superoxide anions into hydrogen peroxide (H_2O_2) and molecular oxygen,[9,10] followed by the reduction of hydrogen peroxide to water (H_2O) by catalase in peroxisomes or glutathione peroxidase in mitochondria.[1,12] Thus, SOD serves as a major antioxidant enzyme responsible for the first step of the superoxide removal system. Recent studies of streptozotocin-induced diabetic rats have shown that chronic hyperglycemia enhance NAD(P)H oxidase activity in kidneys.[4,13,14] Furthermore, we have more recently demonstrated that chronic hyperglycemia causes a reduction of renal SOD expression and activity in a mouse model susceptible to the development of DN.[15] On the basis of these findings, renal alterations of NAD(P)H oxidase and SOD enzymes are likely to be responsible for the renal superoxide excess observed in chronic hyperglycemia.

Angiotensin II is an important vasoconstrictor that regulates systemic and glomerular hemodynamics. In addition, angiotensin II is also known to promote sodium reabsorption, cell growth and extracellular matrix deposition in kidneys.[16] These effects are generally triggered by signaling via angiotensin II type 1 (AT1) receptors.[16] Therefore, AT1 receptor blockade not only improves systemic hypertension but also could provide direct renoprotective effects. Indeed,

[1]Division of Endocrinology, Metabolism and Geriatric Medicine, Akita University Graduate School of Medicine, Akita, Japan; [2]Division of Gastroenterology, Honjo Daiichi Hospital, Akita, Japan and [3]Division of Nephrology, Vanderbilt University Medical Center, Nashville, TN, USA
Correspondence: Dr H Fujita, Division of Endocrinology, Metabolism and Geriatric Medicine, Akita University Graduate School of Medicine, 1–1–1 Hondo, Akita 010-8543, Japan.
E-mail: hirofuji@gipc.akita-u.ac.jp
Received 10 March 2011; revised 21 July 2011; accepted 5 August 2011; published online 10 November 2011

AT1 receptor blockers (ARBs) have been shown to exert greater renoprotective effects in patients with DN than other classes of anti-hypertensive drugs. Clinical studies have reported that irbesartan, an ARB, significantly inhibits the aggravation of renal function in type 2 diabetic patients with overt DN compared with amlodipine,[17] a calcium channel blocker, and that valsartan, another ARB, significantly reduces albuminuria in type 2 diabetic patients with incipient DN compared with amlodipine.[18] It is noteworthy that the renoprotective effects of ARBs were independent of their systemic blood pressure-lowering properties. Recently, evidence for the anti-oxidative effects of ARBs has been accumulating for several members of the ARB class. Clinical studies have reported that ARBs, including losartan, candesartan, olmesartan, telmisartan and valsartan, reduce the urinary levels of oxidative stress marker 8-hydroxy-2′-deoxyguanosine in patients with DN.[19,20] Oxidative stress induced by superoxide excess under chronic hyperglycemia has been thought to be a major factor involved in the pathogenesis of DN.[21] Therefore, the powerful renoprotective properties of ARBs may be attributed to their antioxidative effects.

The role of angiotensin II in modulating superoxide-producing enzyme NAD(P)H oxidase has been explored in vascular cells and kidneys. Previous experimental studies have demonstrated that angiotensin II promotes superoxide generation via NAD(P)H oxidase activation in vascular cells.[22,23] Furthermore, recent experimental studies have indicated that ARBs, such as olmesartan and telmisartan, reduce glomerular superoxide production through downregulating the gene expression of NAD(P)H oxidase subunits p22*phox* and p47*phox* in subtotal nephrectomized rats[24] and catalase-deficient acatalasemic mice.[25] However, whether the angiotensin II signaling and its inhibition modulate the superoxide-scavenging SOD enzymes in kidneys exposed to hyperglycemia is largely unknown.

To investigate whether AT1 receptor blockade alters the expression and activity of SOD enzymes in kidneys exposed to hyperglycemia, we treated non-obese and hypoinsulinemic C57BL/6-*Ins2*^{Akita} (C57BL/6-Akita) diabetic mice with telmisartan, an ARB, or amlodipine, a calcium channel blocker, and compared the effects of these two anti-hypertensive drugs on renal SOD. We report here that telmisartan not only reduces renal NAD(P)H oxidase activity but also upregulates the renal expression and activity of SOD, resulting in a reduction of renal superoxide levels. To explore the mechanism underlying this upregulation of renal SOD with telmisartan, we further examined whether NAD(P)H oxidase inhibition with apocynin modulated the renal expression of SOD and redox-sensitive transcription factor Nrf2 (NF-E2-related factor 2), which is known to upregulate several antioxidant enzymes, including SOD,[26–28] in C57BL/6-Akita diabetic mice.

METHODS

Experimental animals

Male C57BL/6-Akita diabetic and C57BL/6-wild-type (C57BL/6-WT) non-diabetic mice were purchased from SLC (Shizuoka, Japan). The mice were housed (n=3–4 per cage) in a room with a relative humidity of 50% and a 12/12-h light/dark cycle at 20–22 °C, and had unrestricted access to standard rodent chow and water. Animal experiments were conducted in accordance with the Animal Welfare Guidelines of Akita University. All procedures were approved by the Committee on Animal Experimentation of Akita University.

Treatment protocols for telmisartan, amlodipine and apocynin

Telmisartan was kindly provided by Boehringer Ingelheim (Tokyo, Japan). Amlodipine, apocynin (4′-hydroxy-3′-methoxyacetophenone) and carboxymethylcellulose-Na were purchased from Sigma-Aldrich (St Louis, MO, USA). To investigate the effects of telmisartan and amlodipine on renal SOD and NAD(P)H oxidase, 10-week-old male C57BL/6-Akita diabetic mice were administered with telmisartan (5 mg kg^{-1}) orally or amlodipine (5 mg kg^{-1}) dissolved in a 0.5% carboxymethylcellulose-Na solution once daily for 4 weeks. Mice in the control group were given the same volume of 0.5% carboxymethylcellulose-Na solution alone as the vehicle. To examine the effects of NAD(P)H oxidase inhibition on renal SOD, 10-week-old male C57BL/6-Akita diabetic mice were treated with apocynin (40 mg kg^{-1} per day) for 8 weeks. Apocynin was added in the drinking water and was administered orally to the mice as described previously.[29] Mice in the control group were given water alone as the vehicle.

Measurement of blood and urine parameters

Blood glucose was measured using Glucocard Diameter (Arkray, Tokyo, Japan) on samples obtained after a 6-h daytime fast. Blood urea nitrogen, total plasma cholesterol and plasma triglycerides were enzymatically measured by an autoanalyzer (Fuji Dry-Chem 5500, Fuji Film, Tokyo, Japan). Urinary albumin excretion was assessed by determining the albumin-to-creatinine ratio in morning spot urine as previously described.[30] Urine albumin and creatinine were measured by an Albuwell-M Murine Microalbuminuria ELISA kit and a Creatinine Companion kit, respectively (Exocell, Philadelphia, PA, USA).

Measurement of physiological parameters and renal histologic analysis

Systolic blood pressure was measured in conscious trained mice at room temperature using a non-invasive tail cuff and a pulse transducer system (BP-98A, Softron, Tokyo, Japan). The glomerular filtration rate (GFR) was measured by a single-bolus fluorescein isothiocyanate-inulin injection method as described previously.[31] For renal histologic analysis, we stained kidney sections with periodic acid-Schiff (PAS). We used a semi-quantitative score to evaluate the degree and extent of glomerular mesangial expansion as described previously.[30]

Renal superoxide production and activity of NAD(P)H oxidase and SOD

Renal superoxide levels were assessed by dihydroethidium (DHE) histochemistry and a water-soluble tetrazolium salt (WST-1, 2-[4-iodophenyl]-3-[4-nitrophenyl]-5-[2,4-disulfophenyl]-2H-tetrazolium) reduction assay as previously described.[15] The specificity of the WST-1 assay was confirmed by pretreating 10 mg of kidney tissue with polyethylene glycol-SOD (20U; Sigma-Aldrich) overnight at 37 °C. Renal superoxide levels were expressed as the absorbance at 450 nm per 10 mg tissue. For the DHE staining, we examined the Eth-DNA fluorescence at 480 nm excitation and 610 nm emission. To measure renal NAD(P)H oxidase and SOD activity, we prepared kidney lysates using phosphate-buffered saline-perfused and freshly removed renal cortical tissue as previously described.[15] Renal NAD(P)H oxidase activity was measured by a lucigenin-enhanced chemiluminescence assay as previously described.[14] Renal SOD activity was determined using an SOD assay kit-WST (Dojindo Molecular Technologies, Gaithersburg, MD, USA) as previously described.[15] The protein amount was measured using a bicinochoninic acid protein assay (Sigma-Aldrich). The enzymatic activity of NAD(P)H and SOD were expressed in relative chemiluminescence (light) units (RLU) per 100 μg protein and units per mg protein, respectively.

Western blot analysis and immunohistochemistry

For western blot analysis, the kidney lysate prepared for the SOD activity measurement was used. In all, 20 μg of protein was separated by SDS-PAGE and subjected to immunoblots. As the primary antibody, we used rabbit anti-CuZn-SOD (SOD1) (1 : 10 000; Stressgen, Ann Arbor, MI, USA), anti-Mn-SOD (SOD2) (1 : 10 000; Stressgen), anti-EC-SOD (SOD3) (1 : 2000; Stressgen) or anti-Nrf2 (1 : 1000; Santa Cruz Biotechnology, Santa Cruz, CA, USA) polyclonal antibodies. The loading of lysate protein was evaluated by an immunoblot using rabbit anti-actin antibody (1 : 1000; Sigma-Aldrich). The intensity of the signals was semi-quantified using Adobe Photoshop (version CS4; Adobe Systems, San Jose, CA, USA). For the immunohistochemistry, cryostat sections were prepared as previously described.[15] We labeled the sections with rabbit

Table 1 Physiological and biochemical parameters after 4-week treatment with amlodipine or telmisartan in C57BL/6-Akita diabetic mice

	C57BL/6-WT	*C57BL/6-Akita*		
Parameter	*No treatment*	*Vehicle*	*Amlodipine*	*Telmisartan*
n	8	6	6	8
Body weight (g)	23.6 ± 0.7	20.6 ± 0.6*	19.9 ± 0.4*	20.6 ± 0.5*
Systolic blood pressure (mm Hg)	99 ± 2	116 ± 5*	103 ± 2‡	102 ± 3‡
Blood glucose (mg dl^{-1})	148 ± 8	463 ± 18†	429 ± 19†	447 ± 18†
BUN (mg dl^{-1})	23.6 ± 0.7	32.5 ± 1.9*	33.2 ± 1.9*	32.5 ± 2.2*
Total cholesterol (mg dl^{-1})	76.8 ± 3.6	82.6 ± 2.0	84.8 ± 6.8	82.7 ± 3.4
Triglyceride (mg dl^{-1})	75.0 ± 4.4	75.0 ± 4.3	72.7 ± 3.1	69.6 ± 4.7
Urinary albumin (μg per mg creatinine)	9.4 ± 4.8	59.2 ± 6.7†	56.9 ± 5.6†	28.6 ± 3.9§
GFR (ml min^{-1} per g BW)	10.0 ± 0.5	16.3 ± 1.1†	16.7 ± 0.9†	12.7 ± 0.4‡
LKW/BW (g kg^{-1})	7.2 ± 0.3	11.5 ± 0.4†	11.9 ± 0.5†	9.4 ± 0.2†,§
Mesangial expansion score	0.15 ± 0.01	0.44 ± 0.03†	0.41 ± 0.05†	0.40 ± 0.03†

Abbreviations: BUN, blood urea nitrogen; BW, body weight; GFR, glomerular filtration rate; LKW, left kidney weight.
Values are means ± s.e.m. *$P<0.01$, †$P<0.001$ *vs.* C57BL/6-WT. ‡$P<0.05$, §$P<0.01$ *vs.* vehicle.

anti-CuZn-SOD (SOD1) (1 : 100; Stressgen), anti-Mn-SOD (SOD2) (1 : 100; Stressgen) or anti-EC-SOD (SOD3) (1 : 50; Stressgen) polyclonal antibodies for 1 h at room temperature, followed by Alexa Fluor 488-conjugated goat anti-rabbit IgG antibody (1 : 200; Molecular Probes, Eugene, OR, USA) for 30 min at room temperature. We then counterstained the sections with ToPro-3 (Molecular Probes).

Measurement of renal prostaglandin E2 (PGE2) levels

Renal PGE2 levels were measured using freshly isolated renal cortical tissue as previously described.[32] The levels were expressed as the ratio of renal cortical PGE2 to protein.

Statistical analysis

Data were presented as the mean ± s.e.m. Statistical analyses were conducted using GraphPad Prism software (GraphPad, San Diego, CA, USA). Differences between groups were determined by an unpaired *t*-test or a one-way ANOVA, followed by Bonferroni's multiple comparison test. A $P<0.05$ was considered statistically significant.

RESULTS

Biochemical and physiological parameters, and renal histopathology after a 4-week treatment with telmisartan or amlodipine in C57BL/6-Akita diabetic mice

Table 1 shows the biochemical and physiological parameters after a 4-week treatment with telmisartan or amlodipine in C57BL/6-Akita diabetic mice. Data from telmisartan-treated mice were compared with those from the mice treated with amlodipine. Treatment with either telmisartan or amlodipine did not affect blood glucose, body weight, blood urea nitrogen, total cholesterol or triglyceride levels. Compared with the vehicle-treated mice, both amlodipine-treated and telmisartan-treated mice exhibited significantly lower blood pressure levels. There were no significant differences in blood pressure levels between amlodipine-treated and telmisartan-treated mice. Compared with the data from vehicle-treated mice, treatment with telmisartan significantly reduced urinary albumin levels, GFR, and the left kidney weight-to-body weight ratio (LKW/BW) in C57BL/6-Akita diabetic mice, whereas treatment with amlodipine had no effect. As we recently reported, glomerular pathological damages were relatively mild in 10–15-week-old C57BL/6-Akita diabetic mice.[15] A difference in glomerular pathological changes evaluated using the mesangial expansion score was not observed between vehicle-treated and telmisartan-treated C57BL/6-Akita diabetic mice.

Effects of treatment with telmisartan on renal superoxide production, NAD(P)H oxidase activity and SOD activity in C57BL/6-Akita diabetic mice

Figure 1 shows renal superoxide production, NAD(P)H oxidase activity and SOD activity after a 4-week treatment with telmisartan or amlodipine in C57BL/6-Akita diabetic mice. Renal superoxide levels were assessed by DHE histochemistry and a WST-1 assay. The DHE fluorescence signal, which reflects superoxide production, was decreased in the glomeruli of telmisartan-treated C57BL/6-Akita diabetic mice compared with vehicle-treated mice (Figure 1A). Furthermore, telmisartan but not amlodipine significantly reduced renal superoxide levels as determined by the WST-1 assay in C57BL/6-Akita diabetic mice (Figure 1B). Consistent with a recent report,[33] telmisartan reduced NAD(P)H activity in the kidneys of C57BL/6-Akita diabetic mice close to the levels of C57BL/6-wild-type (C57BL/6-WT) non-diabetic mice (Figure 1C). Interestingly, telmisartan-treated C57BL/6-Akita diabetic mice but not amlodipine-treated mice showed significantly higher renal SOD activity than the vehicle-treated mice (Figure 1D). Thus, it should be noted that two telmisartan-treated and amlodipine-treated C57BL/6-Akita diabetic mouse groups exhibited different levels of renal NAD(P)H and SOD activity, despite comparable levels of hyperglycemia and blood pressure.

Effects of treatment with telmisartan on the renal expression of SOD isoforms and Nrf2 in C57BL/6-Akita diabetic mice

We next examined whether a 4-week treatment with telmisartan affected the renal expression of SOD isoforms and Nrf2. Western blot analysis revealed increased expression of the SOD isoforms SOD1, SOD2, and SOD3 and Nrf2 in the renal cortex of telmisartan-treated C57BL/6-Akita diabetic mice, whereas renal SOD and Nrf2 upregulation was not observed in amlodipine-treated mice (Figure 2). Figure 3 shows the renal SOD isoform expression using immunofluorescence histochemistry. As shown in our recent report,[15] SOD1 and SOD2 were broadly expressed in glomerular and tubular cells (tubular SOD1 expression not shown). SOD3 expression was observed in glomerular capillaries and the arteriolar wall (expression of SOD3 in the arteriolar wall not shown). Consistent with the results of the western blot analysis, strong SOD1 and SOD3 signals in the glomeruli and SOD2 signals in proximal tubules were observed in telmisartan-treated C57BL/6-Akita diabetic mice.

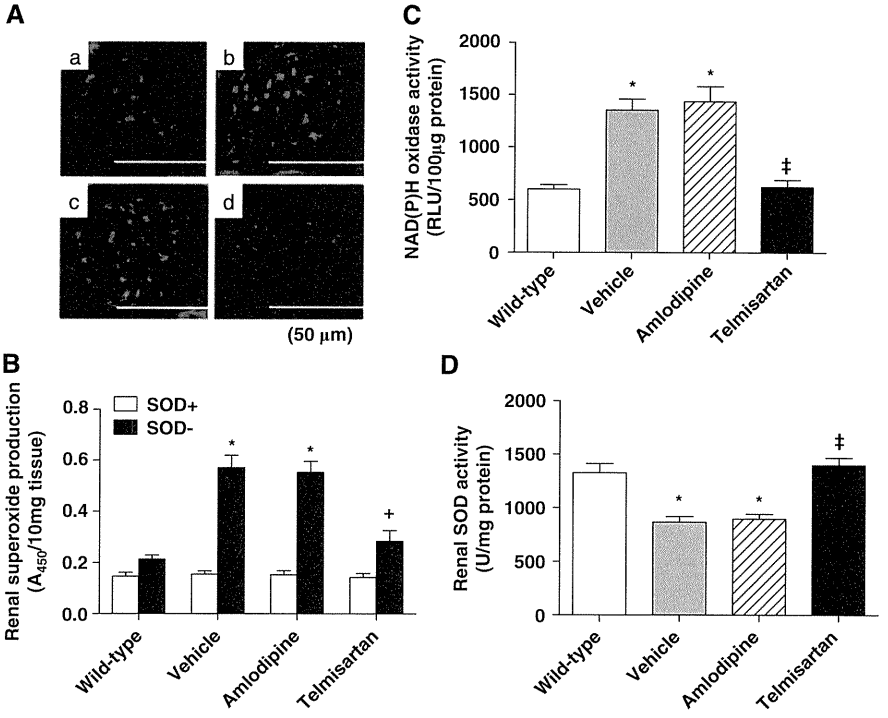

Figure 1 Effects of telmisartan treatment on renal superoxide production, NAD(P)H oxidase activity and SOD activity in C57BL/6-Akita diabetic mice. The C57BL/6-Akita diabetic mice were treated with the vehicle, amlodipine or telmisartan for 4 weeks. The treatment started at 10 weeks of age and ended at 14 weeks of age. The data from C57BL/6-Akita diabetic mice were compared with those from age-matched C57BL/6-wild-type non-diabetic mice. (**A**) Representative glomerular DHE staining after a 4-week treatment with telmisartan. (a) C57BL/6-wild-type; (b) vehicle-treated C57BL/6-Akita; (c) amlodipine-treated C57BL/6-Akita; (d) telmisartan-treated C57BL/6-Akita. (**B**) Renal superoxide production after a 4-week treatment with telmisartan. Data are presented as the mean ± s.e.m. SOD+, kidney tissue pre-incubated with SOD-PEG protein; SOD−, kidney tissue without SOD-PEG protein. n=5 per group. $^{*}P<0.001$ *vs.* wild-type. $^{+}P<0.01$ *vs.* vehicle. (**C**) Renal NAD(P)H oxidase activity after a 4-week treatment with telmisartan. Data are presented as the mean ± s.e.m. n=5 per group. $^{*}P<0.001$ *vs.* wild-type. $^{\ddagger}P<0.001$ *vs.* vehicle. (**D**) Renal SOD activity after a 4-week treatment with telmisartan. Data are presented as the mean ± s.e.m. n=5 per group. $^{*}P<0.001$ *vs.* wild-type. $^{\ddagger}P<0.001$ *vs.* vehicle.

In contrast, the kidneys of amlodipine-treated C57BL/6-Akita diabetic mice did not exhibit increased expression of SOD isoforms.

NAD(P)H oxidase inhibition by treatment with apocynin and renal alterations of the SOD enzyme and Nrf2 in C57BL/6-Akita diabetic mice

We found that telmisartan reduced renal superoxide levels through downregulating NAD(P)H oxidase and upregulating SOD in a mouse model of diabetes, C57BL/6-Akita mice. To explore whether NAD(P)H oxidase regulates the SOD enzyme via Nrf2 in kidneys, we treated C57BL/6-Akita diabetic mice with apocynin, an NAD(P)H oxidase inhibitor, for 8 weeks and investigated the renal alterations of the SOD enzyme and Nrf2. As shown in Table 2, apocynin treatment did not affect body weight, blood pressure, blood glucose or LKW/BW. As expected, a marked reduction of renal superoxide and NAD(P)H oxidase activity was observed in the apocynin-treated C57BL/6-Akita diabetic mice. In addition, apocynin significantly lowered urinary albumin levels and ameliorated elevated GFR in C57BL/6-Akita diabetic mice. Figure 4 shows the western blot analysis of renal cortical expression of SOD isoforms and Nrf2 after an 8-week treatment with apocynin. Interestingly, renal cortical expression levels of SOD1, SOD2 and SOD3 isoforms and Nrf2 were significantly increased in apocynin-treated C57BL/6-Akita diabetic mice compared with vehicle-treated mice.

Effects of telmisartan and apocynin on renal production of vasodilatory PGE2 in C57BL/6-Akita diabetic mice

To elucidate the mechanism through which superoxide reduction due to treatment with telmisartan or apocynin affects glomerular hemodynamics, we measured renal cortical levels of vasodilatory PGE2, which contributes to the development of glomerular hypertension in C57BL/6-Akita diabetic mouse groups treated with telmisartan for 4 weeks and with apocynin for 8 weeks. As shown in Figure 5, a reduction of renal PGE2 production was observed in the telmisartan-treated and apocynin-treated groups compared with the vehicle-treated group.

DISCUSSION

Telmisartan is a unique ARB with peroxisome proliferator-activated receptor-γ activity,[34] and this ARB has been reported to offer a more powerful antioxidative effect than other members of the ARB class in patients with DN.[20] In this study, we first treated 10-week-old C57BL/6-Akita diabetic mice with telmisartan for 4 weeks and investigated whether AT1 receptor blockade by telmisartan modulated the superoxide-scavenging SOD enzyme in kidneys exposed to hyperglycemia. C57BL/6-Akita mice are well-characterized as a model of non-obese and hypoinsulinemic diabetes, and develop marked hyperglycemia as early as 4 weeks of age because of a single mutation in cysteine 96 to tyrosin in the insulin 2 gene (*Ins2*^{Akita}).[35,36] Chemicals such as streptozotocin or alloxan are widely used to induce diabetes in

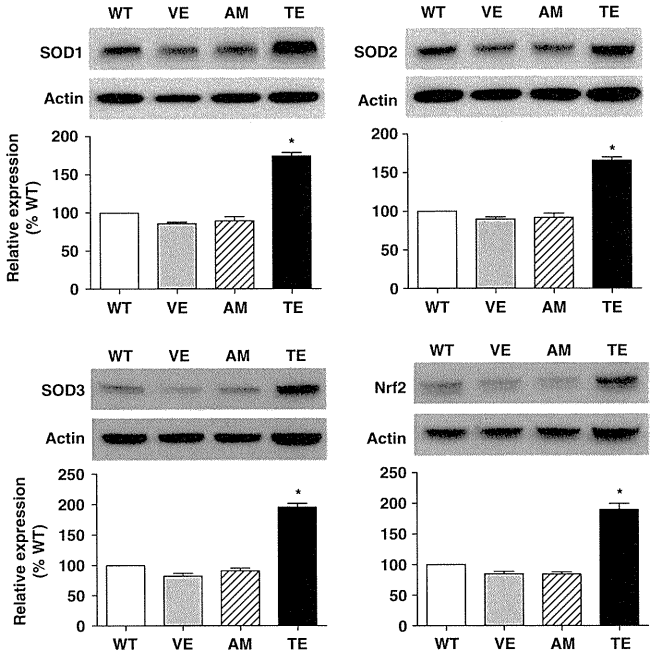

Figure 2 Western blot analysis of renal cortical SOD isoforms and Nrf2 expression after a 4-week treatment with the vehicle (VE), amlodipine (AM) or telmisartan (TE) in C57BL/6-Akita diabetic mice. WT indicates non-diabetic C57BL/6-wild-type mice. The relative intensity of the SOD-to-actin or Nrf2-to-actin ratios to WT is also shown in the lower panels. Data are presented as the mean ± s.e.m. n=4 per group. $^{*}P<0.001$ *vs.* VE.

experimental animals. However, these chemicals have been documented to generate reactive oxygen species and enhance oxidative stress.[37] Therefore, the C57BL/6-Akita mouse model offers a unique opportunity to precisely assess the renal alterations of oxidative stress and its related enzymes.

Consistent with the results of clinical studies,[17,18] our data also indicate that an ARB, telmisartan, is superior to a calcium channel blocker, amlodipine, at producing renoprotective effects in C57BL/6-

Table 2 Physiological and biochemical parameters after 8-week treatment with apocynin in C57BL/6-Akita diabetic mice

Parameter	*Vehicle*	*Apocynin*
n	5	5
Body weight (g)	23.0 ± 0.4	23.4 ± 0.4
Systolic blood pressure (mm Hg)	116 ± 2	115 ± 4
Blood glucose (mg dl^{-1})	466 ± 18	474 ± 7
Urinary albumin (μg per mg creatinine)	66.4 ± 5.8	32.7 ± 4.6*
GFR (ml min^{-1} per g BW)	16.9 ± 0.8	12.2 ± 0.7*
LKW/BW (g kg^{-1})	10.3 ± 0.5	9.3 ± 0.4
Renal superoxide (A_{450}/10 mg tissue)	0.609 ± 0.023	0.244 ± 0.023†
Renal NAD(P)H oxidase activity (RLU per 100 μg protein)	1236 ± 16	315 ± 20†
Renal SOD activity (U mg^{-1} protein)	824 ± 34	1285 ± 78†

Abbreviations: BW, body weight; GFR, glomerular filtration rate; LKW, left kidney weight; RLU, relative light units; SOD, superoxide dismutase.
Values are means ± s.e.m. *P<0.01, †P<0.001 *vs.* vehicle.

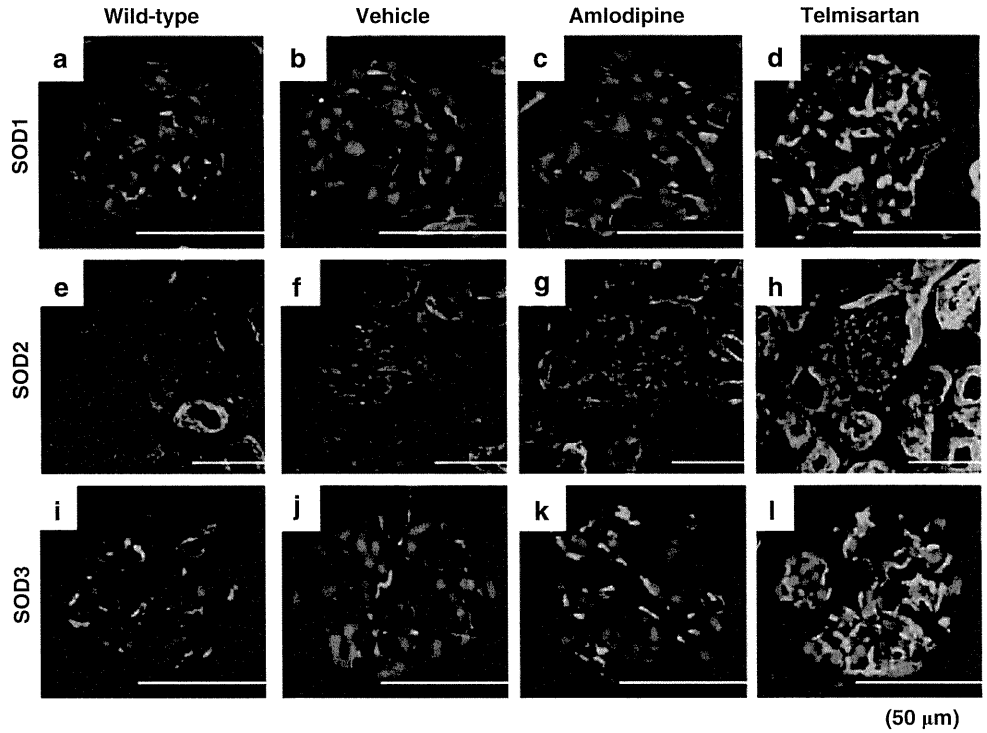

Figure 3 Immunofluorescence SOD isoform staining of kidney sections after a 4-week treatment with the vehicle, amlodipine or telmisartan in C57BL/6-Akita diabetic mice. (**a**–**d**) SOD1; (**e**–**h**) SOD2; (**i**–**l**) SOD3; (**a**, **e**, **i**) C57BL/6-wild-type; (**b**, **f**, **j**) vehicle-treated C57BL/6-Akita; (**c**, **g**, **k**) amlodipine-treated C57BL/6-Akita; (**d**, **h**, **l**) telmisartan-treated C57BL/6-Akita.